NTNU
Norwegian University of
Science and Technology

Macro-model description and model verification

Marius Mathisen Søvik

Civil and Environmental Engineering
Submission date: June 2017
Supervisor: Gudmund Reidar Eiksund, IBM
Co-supervisor: Joar Tistel, IBM

Norwegian University of Science and Technology
Department of Civil and Environmental Engineering

NORWEGIAN UNIVERISTY OF SCIENCE AND TECHNOLOGY-
DEPARTMENT OF CIVIL AND ENVIRONMENTAL ENGINEERING

Report Title: Macromodel Description and Model Verification	**Date**: **11.06.2017** **Number of pages: 96** Master Thesis x
Name: Marius Mathisen Søvik	
Professor in charge/supervisor: Gudmund Reidar Eiksund (NTNU)	
Other supervisors: Joar Tistel (NTNU) and Gustav Grimstad (NTNU)	

Abstract:

The interaction between structures and soil is often idealized to simplify the problem. However, the soil structure interaction (SSI) is important for accurately predicting the mechanical behavior of foundations. Through the framework of macro-modelling, the SSI can be described within a single macro-element. The macro-element can be coupled with the structural analysis, thus simplifying the analysis and saving computational time.

The model presented is described with three degrees of freedom and based on plasticity-theory. The macro-model is calibrated with finite elements. Validation is done with the use of a small scale-foundation tested on medium grained and medium dense sand. This sand is subject to index- and triaxial testing to get representative parameters for the Hardening Soil-model used for calibration.

The performance of the macro-model and its applicability for a shallow foundation anchoring large eccentric forces are investigated. Comparison shows that the model is able to reproduce the mechanical behavior quite well and is deemed satisfactory for describing the behavior of the foundation, although some modifications are suggested. The mechanical behavior is somewhat stiff (attributed to a high shear modulus) and the capacity in the M/B-H plane is slightly underestimated.

Stikkord:

1. Macro model
2. Soil structure interaction
3. Elasto-plasticity
4. Shallow foundation

Marius Mathisen Søvik

(sign.)

NTNU – Trondheim
Norwegian University of
Science and Technology

MSc Thesis

TBA4900 – Geotechnical Engineering

June 2017

By

Marius Mathisen Søvik

Title: Macro-model Description and Model Verification

BACKGROUND

Bearing capacity is essential for all geotechnical structure. This can be approached by classical formulae, e.g. Terzaghi's bearing capacity formula. Although all standard bearing capacity formulae make some use of the concepts of plasticity theory, they all also employ empirical factors. If a foundation is subject to large eccentric forces, it can be convenient to approach the issue in a general-load space, e.g. (V, M, H) if the problem is of a 2D nature. Plasticity-based analyses can be constructed by using force-resultants and their corresponding displacements to be implemented in the numerical analysis. This is considered a more powerful approach, than e.g. increasing the number of empirical factors.

PROBLEM FORMULATION

The interaction between structure and soil is often idealized to simplify the problem. Elastic springs, or rigid constraints are two such simplifications. However, if the global kinematic behavior of soil can be described in terms of fewer general displacements at the footing, then the problem can be idealized through the concept of macro-modelling.

This MSc work aims to study a macro-model describing the interaction between a foundation subject to large eccentric forces in the (V, M, H) space. The macro-model is calibrated with finite elements and validated with small scale prototype tests at a test facility at NTNU.

Professor in charge:	Co-supervisors:
Gudmund Reidar Eiksund (NTNU)	Joar Tistel (NTNU) and Gustav Grimstad (NTNU)

Department of Civil and Environmental Engineering, NTNU

Gudmund Eiksund

Professor in charge

Preface

This is a master thesis in geotechnics at NTNU as a part of the MSc in Civil and Environmental Engineering, carried out during the spring semester of 2017.

This has been a very interesting semester. The subject is of great interest, and I've been lucky enough to do a wide range of practical hands-on tasks, from which I have learned a lot.

Trondheim, 2017-06-11

Marius Mathisen Søvik

Marius Mathisen Søvik

Acknowledgment

The work presented herein have been dependent on many contributors, without whom the final product would never have reached this stage. Firstly, I would like to thank Joar Tistel for the interesting discussion we've had throughout this last semester. Without the preparatory work and presented macro-model associated with his pHD, this thesis could not have gone so smoothly. The MATLAB-script on which the macro-model is dependent is written by Joar Tistel and Gustav Grimstad. I've had many interesting discussions with Gustav, whose help has been appreciated.

I'd like to thank Frank Stæhli, Espen Andersen, Karl Ivar Volden Kvisvik and Ashenafi Lulseged Yifru for their help concerning the preparations for the prototype-testing. I'd also like to thank Per Asbjørn Østensen, who did the necessary preparations in the commercial software LabView, used for the load-control during the prototype-testing.

Although the test-equipment for triaxial testing on sand was a bit crude, eventually some tests were successful, and without the help of Arnfinn Emdal this wouldn't have been possible. In addition, the guidance of Rune Dyvik at the Norwegian Geotechnical Institute (NGI) was appreciated when discussing the moist-tamping technique used for triaxial sample-preparation.

I would especially like to thank Gudmund Eiksund, with whom I've kept close communication throughout my thesis. He's been very helpful and supporting, always available, always willing to answer questions and to discuss my results.

M.M.S.

Abstract

The interaction between structures and soil is often idealized to simplify the problem. However, the soil structure interaction (SSI) is important for accurately predicting the mechanical behavior of foundations. Through the framework of macro-modelling, the SSI can be described within a single macro-element. The macro-element can be coupled with the structural analysis, thus simplifying the analysis and saving computational time.

The model presented is described with three degrees of freedom and based on plasticity-theory. The macro-model is calibrated with finite elements. Validation is done with the use of a small scale-foundation tested on medium grained and medium dense sand. This sand is subject to index- and triaxial testing to get representative parameters for the Hardening Soil-model used for calibration.

The performance of the macro-model and its applicability for a shallow foundation anchoring large eccentric forces are investigated. Comparison shows that the model is able to reproduce the mechanical behavior quite well and is deemed satisfactory for describing the behavior of the foundation, although some modifications are suggested. The mechanical behavior is somewhat stiff (attributed to a high shear modulus) and the capacity in the M/B-H plane is slightly underestimated.

Sammendrag

Interaksjonen mellom jord og struktur er ofte idealisert for å forenkle problemet. Uansett, så er jord-struktur interaksjonen viktig for å forutse den mekaniske oppførselen av fundamenter. Gjennom makro-modell konseptet, kan jord-struktur interaksjonen bli beskrevet med et enkelt makro-element. Deretter kan makro-elementet bli integrert i struktur-analysen, for så å forenkle analysen betraktelig og spare beregningstid.

Den presenterte modellen er beskrevet med tre frihetsgrader basert på plastisitetsteori. Makro-modellen er kalibrert med elementmetoden. Validering er gjort med bruken av et småskala fundament som er testet på sand med middels pakningsgrad og medium kornstørrelse. Denne sanden er så indeks- og triaksial testet for å få representative parametere for Hardening Soil-modellen brukt til kalibrering.

Hvorvidt modellen er i stand til å gi gode resultater og dens anvendbarhet for et overflate-fundament som forankrer store eksentriske krefter er studert. Sammenligning viser at modellen er i stand til å gjengi den mekaniske oppførselen nøyaktig, selv om et par modifikasjoner er foreslått. Den mekaniske oppførselen er litt stiv (grunnet en høy skjær-modulus) og kapasiteten er noe undervurdert i M/B-H planet.

Contents

Chapter 1

Introduction

1.1 Background

For a geotechnical engineer the bearing capacity of soil is of utmost importance. With the development of more sophisticated and powerful computers the use of finite elements has become important for accurate prediction of the mechanical behavior of foundations.

Soil structure interaction(SSI) is the process which describes how the structure influences the adjacent soil, and vice versa. Despite sophisticated computers, SSI analyses can be time-consuming. Regardless of how the structural and geotechnical analyses are incorporated into one another, the design process requires close collaboration between the geotechnical and the structural engineer. Thence, the issue of accurate interaction can be approached through the framework of a so-called macro-model. Such models are able to describe the global behavior of soil in one element, a macro-element, consequently simplifying the analysis.

Jack-up units, spud-can footings and bridge foundations subject to large eccentric forces are examples of common application. If the macro-model is able to reproduce the mechanical behavior of soil sufficiently, then incorporation into a structural analysis is useful. The reduction in degrees of freedom and better control of the structural response are some of the key advantages. By following the generalized load paths one can analyze which kind of structural response is associated with which foundation-response. The applicability of a macro-element describing the SSI between a suspension bridge anchor block foundation and the adjacent soil is investigated.

A better understanding of the theory of macro-modelling will be the platform of this thesis.

1.2 Objectives

The main objective of this thesis is to describe the mechanical behavior of a shallow foundation subject to vertical-, moment- and horizontal loading with a macro-model formulation. In order to do so, the approach is as follows.

1. Describe a constitutive relation for the macro-model
2. Calibrate the macro-model using finite elements
3. Validate the macro-model by use of small scale prototype-tests

1.3 Structure of the Report

The thesis is structured as follows.

- **Chapter 2:** The different concepts evaluated for the crossing at Bjørnafjorden are presented.
- **Chapter 3:** The most relevant theory will be given. This includes bearing capacity, an introduction to plasticity-theory, the outline of the Hardening Soil-model and finally the macro-model formulation.
- **Chapter 4:** The prototype-testing facilities and test-procedures are presented.
- **Chapter 5:** The procedures and results of index- and triaxial tests of the model-sand, on which the small scale prototype-foundation will stand, are presented.
- **Chapter 6:** The results obtained from the finite element analysis are presented, and on the basis of these the calibration of the macro-model is done.
- **Chapter 7:** The results obtained using the prototype-foundation will be compared to those of the macro-model.
- **Chapter 8:** The conducted studies are discussed, summarized and suggestions for further work are given.

Chapter 2

Application at Bjørnafjorden

The E39 Coastal Highway Route on the Norwegian western coast stretches from Kristiansand to Trondheim and is about 1100 km long. It is necessary to cross seven straits by ferry, and the travel time is approximately 21 hours. The national transport plan(NTP) for 2014-2023 states that within 20 years the ferry crossings will be replaced by fixed links. Suspension bridges, submerged tunnels, fixed bridges, floating bridges and combinations of these are all alternatives. By replacing the ferries with fixed links, travel time is estimated to be reduced to 11 hours and the total length reduced by 50 km. By rendering the route ferry-free, the macroeconomic benefits will be in the range between 122 to 373 billion NOK in the period 2013-2060 according to Ulstein et al. (2015).

One of the existing ferry crossings is located just south of Bergen at Bjørnafjorden. Different concepts are considered for this strait crossing, one of which will be examined further in this thesis.

2.1 Topography

Bjørnafjorden is flanked on each side by steep fjord sides, with depths ranging up to 564 m at its deepest, and a width of 5km at the relevant crossing. Anchoring large structures close to the steepest sides of the basin could be troublesome as they can trigger underwater landslides. Moreover, the great depths dominating parts of the strait render the crossing difficult. Technology from the Norwegian off-shore industry has inspired several of the concepts related to the crossing at Bjørnafjorden. In the following is a short presentation of the main-characteristics concerning the evaluated bridge concepts. All of the figures in this chapter are credited to TNPRA (2016).

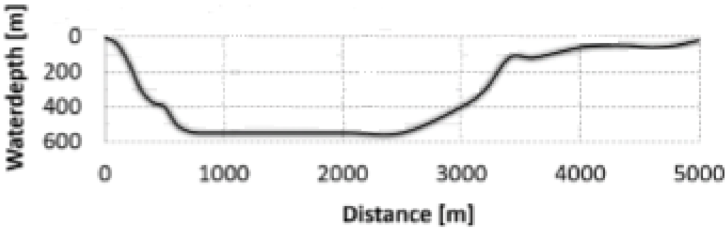

Figure 2.1: Section showing the topography of the fjord-crossing

2.2 Concepts

One proposed solution is a large-span suspension bridge with a main-span more than 3km long. This would make it the bridge with the longest span in the world. The longest span is 1991 m for the Akashi Kaikyō Bridge in Japan, which was completed in 1998 .

Another concept considered is a Submerged Floating Tube Bridge (SFTB), which is a concrete tunnel floating about 20 m below the water surface. This could either be anchored to seabed, or connected to floating pontoons, as seen in Figure 2.2(a).

Floating bridges of lengths more than 5000m are also studied. Both a side-anchored and end-anchored system are considered, with Figure 2.2(b) showing the concept with end-anchoring.

(a) SFTB

(b) Floating bridge with ship passing close to shore

Figure 2.2: Two concepts evaluated

Another concept is a multi-span suspension bridge, with three major spans of 1385, 1325 and 1385 m and a total length of about 5200 m from anchorage to anchorage. The two central floating pylons are supported by tension leg platforms (TLPs) at around 500 m deep water. TLPs have been in use since the 1980's, and are common anchoring methods for platforms at depths ranging from approximately 300-1500m.

The south pylon and suspension cable anchorage are placed on shore, while the north pylon and suspension cable anchorage are placed in shallow water. The combination of suspension bridge and the TLP-anchoring system for the pylon towers would make it the worlds first such bridge.

The large suspension cables on the north side are anchored by a gravity based structure(GBS) acting as the foundation. The cables are transferring large eccentric forces which cause large moment- and horizontal forces to the foundation. The focus of this thesis is a model which can explain the interaction between this anchorage system and the adjacent soil stratum in a relatively simple, but precise manner.

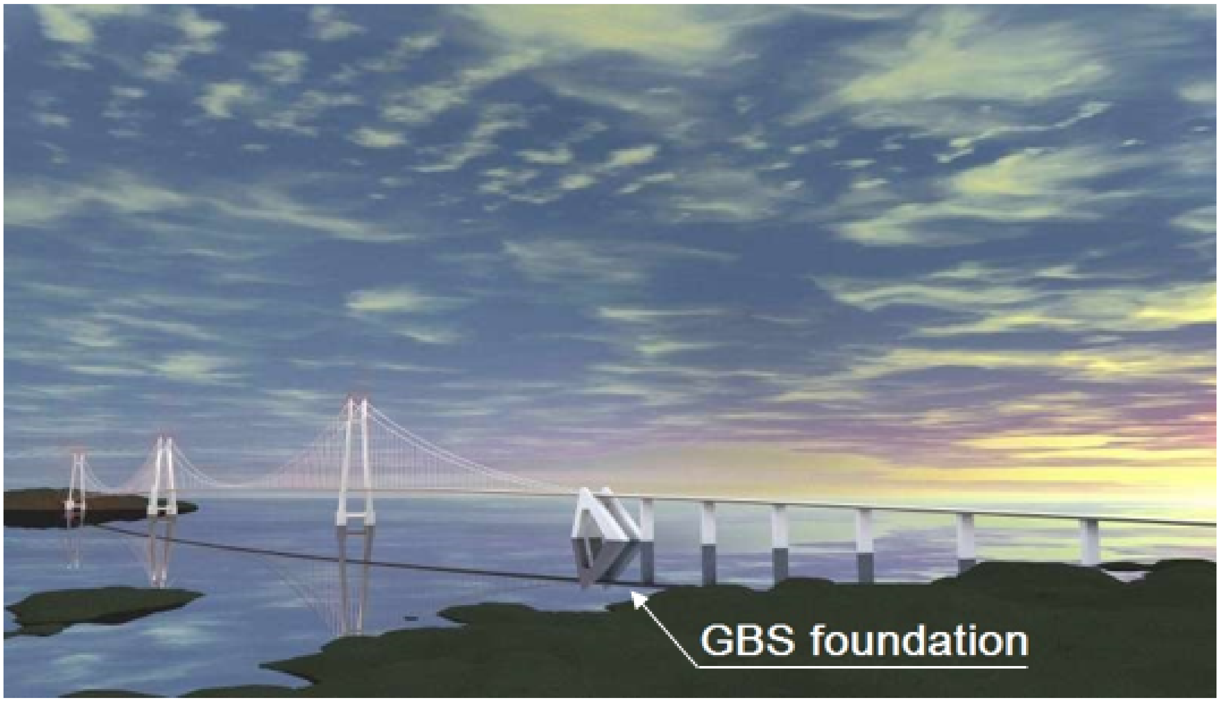

(a) GBS foundation of the bridge shown

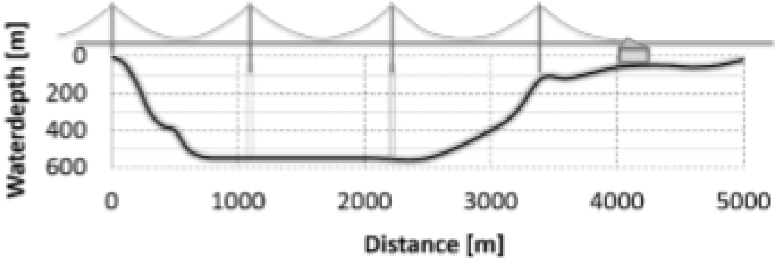

(b) Horizontal section

Figure 2.3: Multi-span suspension bridge concept

Chapter 3

Literature review

The bearing capacity of soil is highly relevant for a geotechnical engineer, and common formulae will be introduced. Moreover, soil can experience elastic and plastic behavior under stress; concepts which are crucial for the understanding of the Hardening Soil-model and the macro-model. The introduction of the macro-model aims at describing complex SSI phenomena in a conceptual easily understood way.

3.1 Bearing capacity

Shallow foundations transfer the loads to the ground at a level close to the surface. The bearing capacity is not a characteristics of either soil or the foundation, but rather the interaction between the two. Depending on the dimensions of the foundation and its major and minor sides(L and B) a shallow foundation can be subdivided into: spread or pad footings(L $\cong$ B); mat, slab or raft foundations; and strip footings(L $\geqslant$ B).

There are three main modes of failure for which a shallow foundations can fail: punching failure(failure due to a local decrease of volume in relative loose soils); general failure(failure due to shearing along a well-defined slip surface); and local failure(an intermediate failure mechanism between punching and general failure). The sand on which the studied prototype-foundation will stand is not considered loose, and therefore only general failure is discussed.

This topic is discussed thoroughly in literature, with Karl von Terzaghi being a pioneer in the field.

3.1.1 Terzaghi's bearing capacity equation

Terzaghi(1943) proposes an equation for the limit value of an uniformly distributed vertical load applied to a horizontal ground surface:

$$Q_{lim}/A = q_{lim} = c \cdot N_c + q \cdot N_q + 0,5 \cdot B \cdot \gamma \cdot N_\gamma \tag{3.1}$$

Whilst the known lateral load is q, the cohesion c, the width of the foundation B and the unit weight of soil γ and a limit load of Q_{lim}. The bearing capacity coefficients N_c, N_q and N_γ are functions of the friction angle and are deduced by the following assumptions:

- Plane strain regime
- Rigid-plastic material behavior
- Limit shear resistance of soil defined by the Mohr Coulomb yield condition
- Principal stress directions at failure coincide with the vertical and horizontal directions
- The bearing capacity coefficients are seperately evaluated on the basis of equilibrium and the Mohr Coulomb failure criterion

If the soil was weightless the three contribution could be superimposed, but the soil is not. The method of characteristics is used in order to approximate N_γ. Thence, N_q and N_c are deduced by a different slip surface than that of N_γ, and superposition will therefore underestimate the maximum bearing capacity in plane strain. These approximations are also done by the two following authors.

3.1.2 Brinch-Hansen's bearing capacity formula

Actual foundations seldom have purely vertical load, are usually placed with a depth D below the surface, have a limited length L and both the foundation base and ground may be inclined. Therefore, Brinch-Hansen (1970) proposes an updated version of Terzaghi's bearing capacity formula:

$$q_{lim} = cN_c s_c d_c i_c b_c g_c + \overline{q} N_q s_q d_q i_q b_q g_q + 0.5 B\gamma N_\gamma s_\gamma d_\gamma i_\gamma b_\gamma g_\gamma \tag{3.2}$$

The introduction of these factors can be derived in a similar manner as with the bearing capacity coefficients; by considering each complication separately and superimposing. The new factors are abbreviated to account for shape(s), depth(d), inclination(i), base inclination(b) and ground inclination(g). In the case of eccentric loading, the eccentricity is taken into consideration by introducing the so-called effective foundation area.

3.1.3 Janbu's bearing capacity formula

Another example of an approximated analytic bearing capacity formula is that of Janbu et al. (1976) based on similar assumptions as Equation 3.1 and 3.2, but with a slightly different formulation. The bearing capacity equation proposed is given as:

$$\overline{\sigma}_v + a = N_q(p^{'} + a) + 0.5N_\gamma\overline{\gamma}B_0 - N_u\overline{u}_b \tag{3.3}$$

The $\overline{\sigma}_v$ is the average stress and $\overline{u}_b$ the average pore pressure over over the effective area B_0, while $\overline{\gamma}$ is the average unit weight of soil. Instead of the bearing capacity coefficient N_c the N_u is utilized, which accounts for the average pore pressure along the effective width of the foundation. Also, the bearing capacity N_γ is deduced in a slightly different manner.

3.2 Theory of elastoplasticity

Thus far only the maximum capacity has been discussed. Now, the relationship between strain and stress will be discussed through the framework of elasto-plasticity. As the theory of both elasticity and plasticity is thoroughly described in literature, only a brief introduction is given in the following. The basic laws necessary for defining any elasto-plastic relationship are (i) an elastic constitutive relationship, (ii) a yield criterion, (iii) a hardening law and (iv) a plastic flow rule.

3.2.1 Elastic constitutive relationship

Elastic behaviour is by definition reversible, i.e. deformation caused by a load is reset to it original state once the load is removed. Such behavior can be both linear and non-linear. The theory of elasticity is incorporated in a constitutive model by Hooke's law, where the relation between incremental stresses and strains are given by:

$$\dot{\boldsymbol{\sigma}} = \boldsymbol{D} \cdot \dot{\boldsymbol{\varepsilon}}^e \tag{3.4}$$

For isotropic elasticity, i.e. material behavior is direction-independent, only two parameters are necessary to describe the elastic constitutive matrix $\boldsymbol{D}$, namely Young's modulus E and Poisson's ratio ν. The dots above the stress vector $\boldsymbol{\sigma}$ and the elastic strain vector $\boldsymbol{\varepsilon}^e$ mean that they are incremental.

3.2.2 Yield criterion

The difference between plastic- and elastic behavior is apparent when an unloading takes place; unlike elastic behavior, permanent strains can occur when unloading plastic. To distinguish between elastic and plastic behavior a yield criterion is introduced. The criterion is given by $F(\boldsymbol{\sigma}, K) = 0$. The criterion is thus dependent on the stress-state of the material and a state variable, here represented by K. K may be a scalar function dependent on e.g. mobilization, or it can be tensorial state variable.

F=0 therefore represents a surface in the stress space, known as the yield surface. In the stress space a stress point can find itself in three states:

1. Elastic behavior when the stress point is located inside the yield surface, F<0.
2. Irreversible strains may develop when the stress point belongs to the yield surface, F=0.
3. The stress point is outside the yield surface, which is inadmissible, F>0.

3.2.3 Hardening law

The way in which the yield surface changes is explained by the hardening law. If a material yields perfectly plastic, then $dF = F(\boldsymbol{\sigma}) = 0$ and no hardening can take place. One such example is the Mohr-Coulomb model. This means that after a certain threshold the material cannot reach a higher state of stress, whilst the yield surface does not change and is independent of loading.

However, most soils can experience hardening behavior. In the following are three examples: (i)isotropic hardening, where the yield surface expands equally in all directions; (ii)kinematic hardening, where the yield surface translates, e.g. by rotation; or(iii) mixed hardening, which means both expansion and translation.

The antagonistic behavior is called softening, where instead a decrease in strength is observed by the material.

The strain hardening law relates the shape, volume and position of the yield surface to the accumulated plastic strains $\boldsymbol{\varepsilon^p}$, with the yield criterion expressed as $F(\boldsymbol{\sigma}, \boldsymbol{\varepsilon^p}) = 0$. When a material is yielding and it is attempted to load the stress state beyond the current yield surface(not admissible) the yield surface expands, i.e. $F(\boldsymbol{\sigma}, \boldsymbol{\varepsilon^p}) = dF(\boldsymbol{\sigma}, \boldsymbol{\varepsilon^p}) = 0$.

The latter condition, namely dF=0, is known as the consistency equation and can further be derived:

$$dF = \frac{\partial F}{\partial \boldsymbol{\sigma}} \cdot d\boldsymbol{\sigma} + \frac{\partial F}{\partial \boldsymbol{\varepsilon^p}} \cdot d\boldsymbol{\varepsilon^p} = 0 \tag{3.5}$$

When hardening takes place plastic strains develop, and to understand how the following is introduced.

3.2.4 Plastic flow rule

The plastic flow rule defines how the plastic strains develop when a state of stress satisfies the following conditions :$F(\boldsymbol{\sigma},\boldsymbol{\varepsilon}^p) = dF(\boldsymbol{\sigma},\boldsymbol{\varepsilon}^p) = 0$. An incremental change in plastic strain is then given as:

$$d\boldsymbol{\varepsilon}^p = d\lambda \cdot \frac{\partial G}{\partial \boldsymbol{\sigma}} \tag{3.6}$$

The dλ is a scalar known as the plastic multiplier and given by the hardening law, while G is a mathematical formulation called the potential surface. In the plastic regime, the increment of strains depend on the current stress state, through the gradient of the plastic potential. If the potential surface is coinciding with the yield surface, i.e. G=F, then the flow rule is associate. If however G≠F, the flow is non-associate. The flow rule hence describes the potential surface, which in turn describes the nature of plastic strain development.

3.3 Hardening Soil model

There are several models, whose formulation describe the relationship between stresses and strains. Some are more appropriate than others when describing certain phenomena. The Hardening Soil model (henceforth called the HS model) can be useful for simulating the behavior of both stiff and soft soils. For the latter, there is a model called the HS Soft model which better models soft soils. Herein, soft soils behavior is not discussed. In the following are the most important aspects of the HS model.

As the name indicates, the model is useful for describing hardening soils, albeit not being able to reproduce softening behavior. The yield surface expands due to plastic straining. Both shear, or cone (deviatoric loading) and compression, or cap hardening (primary compression in oedometer and isotropic loading) are included in the HS model. When the stress state has reached the maximum deviatoric loading the cone-part of the HS-yield surface is coinciding with that of Mohr-Coulomb.

The reference moduli are the respective moduli for the different loading conditions. The different stiffnesses are dependent on the stress state experienced by the material. In the following is a table summarizing the parameters in the HS model.

Parameter	Explanation
E_{50}^{ref}	The reference secant modulus at 50% deviatoric stress in drained triaxial test.
E_{oed}^{ref}	Reference modulus for primary compression in oedometer conditions.
E_{ur}^{ref}	Reference modulus for unloading/reloading in drained triaxial test
K_0^{nc}	Earth pressure coefficient for normally consolidated material
K_0	Earth pressure coefficient for over consolidated material
φ, ψ, c	Friction angle, dilatancy angle and cohesion at failure
v_{ur}	Poisson' ratio for unloading/reloading. Often 0.2.
e_{init}, e_{min}, e_{max}	Void ratio input for dilatancy cut-off
OCR	Over consolidation ratio
m	Modulus exponent
Rf	$\frac{q_f}{q_a}$, see Figure 3.1.
a	c/$tan\phi$
p_{ref}	100kPa

Table 3.1: Hardening Soil model parameters explained

For bearing capacity problems the strains developing on a slip surface at failure can differ: some areas can experience bigger strains than others; and some can even localize, i.e. theoretically go to infinite. Critical state-theory takes into account the fact that volumetric strains cannot go to infinite in a triaxial apparatus, and this can be accounted for by introducing the dilatancy cut-off parameters e_{init}, e_{min} and e_{max}. Hence, these parameters can lead to a more realistic description of the developing strains.

As the deviatoric load is increased, the soil behaves less stiff. Mathematically this can be described by connecting the strains and deviatoric stresses by a hyperbolic relationship, namely:

$$\varepsilon_1 = \frac{2 - R_f}{2E_{50}} \cdot \frac{q}{1 - q/q_a} \tag{3.7}$$

The secant stiffness is given as $E_{50} = E_{50}^{ref} \left(\frac{\sigma_3' + a}{p_{ref} + a} \right)^m$, and describes the stiffness related to deviatoric loading.

Through the framework of the HS model the mechanical behavior observed in e.g. drained triaxial tests on sand can be reproduced realistically. For further description of the Hardening Soil model, see the Material Models Manual by Plaxis.

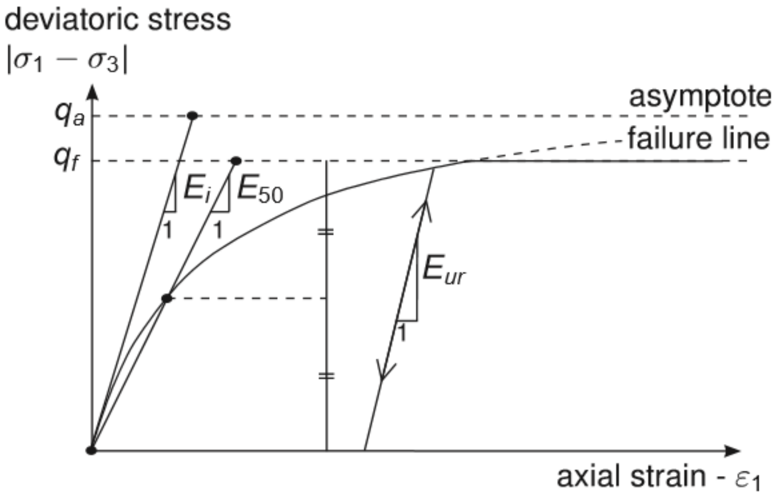

Figure 3.1: Hyperbolic stress-strain relation in primary loading for a standard drained triaxial test(Plaxis)

3.4 The theory of the macro model

3.4.1 Motivation

The bearing capacity formulas of both Terzaghi, Brinch-Hansen and Janbu has been discussed earlier. Even though Brinch-Hansen took eccentric loads into account by introducing the concept of effective area, the formula is still dependent on empirical factors. Such methods might be deemed sufficient for predicting failure, but are not able to pay attention to the development of deformation.

Roscoe and Schofield (1956) was the first who proposed to tackle the issue of bearing capacity directly in the (V, M, H) space. Inspiration was drawn from traditional M-N diagrams for beams, and thence extended to general loading. The problem is then governed by a load combination within a three dimensional space. Different authors have later proposed plasticity based approaches to the problem in the (V, M, H)-space.

For the anchoring foundation in question, large inclined and eccentric forces must be supported. Similar problems are encountered elsewhere, often off shore. Houlsby and Cassidy (2002) approached the issue for jack-up units on sand. Butterfield and Gottardi (1994) did so for shallow footings on sand, while Martin (1994) examined spud-can footings on clay. All had experimental results validating their respective work.

3.4.2 General

The interaction between soil can structure can be idealized in different ways. For example, if the foundation were to stand directly on bedrock, the interaction could be described by rigid constraints. For the sand stratum being considered herein, the rigid constraints or elastic stiffnesses (Winkler springs) can be replaced by a more realistic coupled and non-linear constitutive relationship.

Macro model-theory can be useful to reproduce the mechanical behaviour of large shallow foundations and how they interact with the adjacent soil. It is convenient to substructure the system in two parts: the superstructure, i.e. the bridge; and the soil. Both parts have different materials and mechanical properties. It is convenient to put emphasis on the superstructure, i.e. the bridge, and reduce the amount of degrees of freedom associated with the soil.

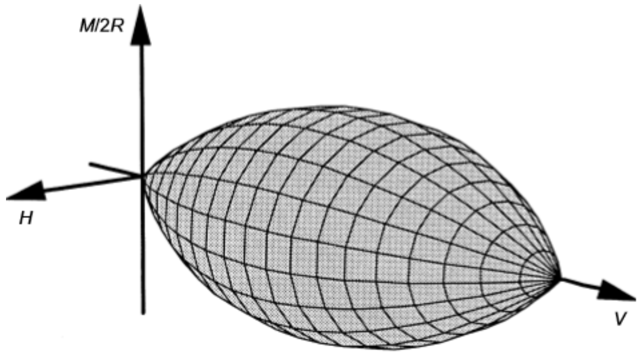

Figure 3.2: Example of yield surface in the V-M/B-H space, by Houlsby and Cassidy (2002)

If the foundation behaves rigidly with respect to the soil, the degrees of freedom of the system can be reduced. Such a hypothesis can reasonably be accepted for large stiff shallow foundations, e.g. large concrete gravity based structures(GBS). Thus, the global soil behaviour and how it interacts with the foundation can be described within one element, a macro-element.

The amount of degrees of freedom associated with the macro-element depends on the loading situation being investigated. Dynamic forces induced by e.g. rough sea are disregarded as they are significantly lower than the static loads acting on the foundation in a two-dimensional plane, as argued by Tistel and Grimstad (2016). Collision loads are not considered herein. If they are to be accounted for in the design, the model can be extended to three-dimensions(6 degrees of freedom).

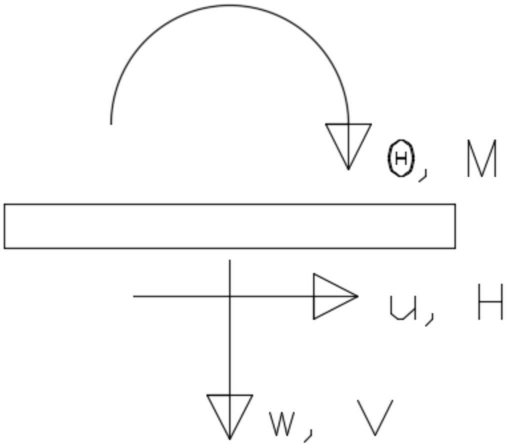

Figure 3.3: Sign convention for displacement and load

Hence, the idealized problem presented is one of three kinematic degrees of freedom: vertical; rotational; and horizontal displacement. These displacements act as generalized strain variables, while the associated forces acts as generalizes stress variables. The forces are denoted as V, M/B and H, and displacements w, B·θ and u. This lead to the following displacement- (**v**) and load-vectors (**S**), with sign convention shown in Figure 3.3. These are working at the bottom centre of the rigid foundation.

$$\mathbf{v}^T = \left[w, \quad B \cdot \theta, \quad u \right], \; \mathbf{S}^T = \left[V, \quad M/B, \quad H \right] \tag{3.8}$$

The aim is to introduce a representative coupled constitutive relationship within a macro-element for the foundation in the finite element-code of the bridge. The methodology used is based on classical plasticity theory with a potential- and yield surface, flow rule and hardening law, all of which will be presented in this chapter.

3.4.3 Yield surface

The nature of the three dimensional yield surface has been paid notable interest in recent years. The yield-surface of Houlsby and Cassidy (2002) is shown in Figure 3.2. On the basis of experiments by Gottardi and Butterfield (1993) the shape of the yield surface in the M/B-H plane(constant V-loading) is suggested as one of a rotated ellipsis. As first pointed out by Zaharescu (1961) the moment and horizontal loads can work either in opposition(-M) or conjunction(+M), and the load case with negative moment (see Figure 3.2 for sign convention) can generate a higher horizontal load for the same magnitude of M. Thus, the rotation of the ellipsis.

Butterfield and Gottardi (1994) presented a three dimensional yield surface based on experimental results in the following form:

$$\left(\frac{H}{h_0}\right)^2 + \left(\frac{M/B}{m_0}\right)^2 - \frac{2 \cdot a \cdot H \cdot M/B}{h_0 \cdot m_0} = \left[\frac{V}{V_{max}} \cdot (V_{max} - V)\right]^2 \tag{3.9}$$

The h_0 and m_0 are the peak horizontal- and moment forces in the V-H and V-M/B planes respectively, divided by V_{max}. Therefore, the shape of the yield surface can be modified in the V-H and V-M planes separately to fit the observed behavior. The introduction of the factor ”a” accounts for the rotated ellipse in the M/B-H plane.

Experimental results conducted by Nova and Montrasio (1991) suggested that the maximum horizontal-, or moment loading in the V-H or V-M/B planes could occur at a load different from $V = 0.5V_{max}$, and closer to V_{max}. Such a shift of the peak-values could be accounted for by introducing a β-value. Furthermore, it was proposed by Martin (1994) that such peaks in the V-H and V-M plane could also occur when V was less than $0.5V_{max}$ and therefore introduced a second β-value. The two values are henceforth referred to as β_1 and β_2. For example, the reduction of β_1 will make the yield-surface lean towards zero vertical force. The β-values also affect the magnitude of the peaks, so in order to preserve the desired peaks μ is introduced:

$$\mu = \frac{(\beta_1 + \beta_2)^{(\beta_1 + \beta_2)}}{\beta_1^{\beta_1} \cdot \beta_2^{\beta_2}} \tag{3.10}$$

The suggested form of the yield surface according to Martin (1994) is:

$$F = \left(\frac{H}{h_0 \cdot V_0}\right)^2 + \left(\frac{M/B}{m_0 \cdot V_0}\right)^2 - \frac{2 \cdot a \cdot H \cdot M/B}{h_0 \cdot m_0 \cdot V_0^2} - \mu^2 \cdot \left(\frac{V}{V_0}\right)^{2\beta_1} \cdot \left(1 - \frac{V}{V_0}\right)^{2\beta_2} = 0 \tag{3.11}$$

It can be convenient to have separate parameters describing the observed behavior in the V-H and V-M/B planes respectively. Therefore, the aforementioned β- and μ-values are henceforth separated to β_{1h}, β_{2h}, μ_h, β_{1m}, β_{2m} and μ_m. The subindices h and m are used for better fit in the V-H and V-M/B planes respectively.

The V_0 presented in the yield surface-formulation above is the so-called mobilized vertical load. The mobilized vertical load is $V_0 = \kappa \cdot V_{max}$. The mobilization is defined by the state parameter κ, which will be examined further when looking at the hardening law.

The final formulation of the yield locus becomes, as defined by Tistel and Grimstad (2016):

$$F = H_F^2 + M_F^2 - N_F^2 - V_F^2 = 0 \tag{3.12}$$

Where:

- $H_F^2 = \left(\frac{H}{h_0 \cdot V_0}\right)^2 \cdot \left(\frac{\mu_m}{\mu_h}\right)^2 \cdot \left(\frac{V}{V_0}\right)^{2(\beta_{1m}-\beta_{1h})} \cdot \left(1 - \frac{V}{V_0}\right)^{2(\beta_{2m}-\beta_{2h})}$
- $M_F^2 = \left(\frac{M/B}{m_0 \cdot V_0}\right)^2$
- $N_F^2 = \frac{2 \cdot a \cdot H \cdot M/B}{h_0 \cdot m_0 \cdot V_0^2} \cdot \frac{\mu_m}{\mu_h} \cdot \left(\frac{V}{V_0}\right)^{(\beta_{1m}-\beta_{1h})} \cdot \left(1 - \frac{V}{V_0}\right)^{(\beta_{2m}-\beta_{2h})}$
- $V_F^2 = \mu_m^2 \cdot \left(\frac{V}{V_0}\right)^{2\beta_{1m}} \cdot \left(1 - \frac{V}{V_0}\right)^{2\beta_{2m}}$

3.4.4 Elasticity

As long as the load combination is within the yield surface the mechanical response is assumed elastic, which calls for a representative elastic constitutive relationship. If the soil is assumed to act isotropic and elastic, then the elastic stiffness matrix is dependent on only two elastic soil properties (shear modulus G and Poisson' ratio), and the foundation geometry(represented by width B).

The incremental elastic constitutive relationship is given in Equation 3.14. The elastic shear modulus is $G = E/2(1+v)$, while B is the major side of the rectangular foundation and the stiffness coefficients $k_{1...4}$ are all dimensionless.

$$\begin{bmatrix} dV \\ dM/B \\ dH \end{bmatrix} = GB \begin{bmatrix} k_1 & 0 & 0 \\ 0 & k_2 & k_4 \\ 0 & k_4 & k_3 \end{bmatrix} \begin{bmatrix} dw^e \\ B \cdot d\theta^e \\ du^e \end{bmatrix} \tag{3.13}$$

Further, by assuming an elastic homogeneous half-space, as first defined by Boussinesq, one can analytically obtain the analytic elastic stiffness terms for circular foundations. However, due to the lack of cylindrical symmetries for rectangular surface foundations no analytic expressions are available. In the literature there has been several approximations for the stiffness terms.

Cremer et al. (2002) conclude that the cross coupling term between the vertical and rotational movement is negligible for a surface foundation. For an infinite elastic half space, the horizontal-rotational cross-coupling is small, but not zero. For the case of limited depth until a stiffer medium than the soil, such a cross coupling term is insignificantly small. However, according to Pais and Kausel (1988) all the cross coupling terms are ”small for a surface foundation". The remaining diagonal stiffnesses can be expressed e.g. on the form by Pais and Kausel($L/B > 1$):

$$k_1 = \frac{GB}{1-\upsilon} \cdot \left(3.1\left(\frac{L}{B}\right)^{0.75} + 1.6\right) \tag{3.14}$$

$$k_2 = \frac{GB^3}{1-\upsilon} \cdot \left(3.73\left(\frac{L}{B}\right)^{2.4} + 0.27\right) \tag{3.15}$$

$$k_3 = \frac{GB}{2-\upsilon} \cdot \left(6.8\left(\frac{L}{B}\right)^{0.65} + 2.4\right) \tag{3.16}$$

3.4.5 Hardening law

The hardening law presented in the following is governed by isotropic strain-hardening, i.e. the material hardens with the accumulation of plastic displacements. The material hardens isotropically, although being fixed in the origin (V, M/B, H)=(0, 0, 0). The yield surface therefore keeps the same shape, while V_0 increases in the positive direction when the soil hardens. At maximum mobilization the κ is unity and therefore $V_0 = V_{max}$.

There are different approaches to this problem. Martin (1994) proposes that the apex of the yield surface(i.e. V_0) is a function of the accumulated vertical plastic displacement w^p, while Byrne and Houlsby (2001) argue that a closer approximation can be made if the hardening behaviour of the material is defined by all plastic displacements, namely w^p, $B \cdot \theta^p$ and u^p. The importance of each plastic contribution are then weighed with different constants. Such a concept give rise to the following equation for the increment of the combined plastic displacement:

$$dU_p = C_1 \cdot du^p + C_2 \cdot (B \cdot d\theta^p) + dw^p \tag{3.17}$$

The state parameter κ is a function of the combined plastic displacement U_p, and depending on the load combination applied to the foundation the hardenling law can be described in different ways. For example, Tistel and Grimstad (2016) observe that for ratios of H/(M/B) close to 1 the hardening law can be approximated to be bi-linear and given by the following equation:

$$\kappa(U_p) = \kappa_0 + a_h \cdot \frac{U_p}{B} \tag{3.18}$$

Because the plastic displacement U_p is dependent on the variables C_1 and C_2, which in turn are load combination-dependent the goal is to find C_1- and C_2-values representative for all relevant load combinations if this bi-linear hardening formulation is deemed sufficient.

3.4.6 Potential surface

The formulation of the potential surface is constructed in a similar manner as the yield surface and given in the following:

$$Q = H_Q^2 + M_Q^2 - N_Q^2 - V_Q^2 = 0 \tag{3.19}$$

Where:

- $H_Q^2 = \left(\frac{H}{h_{0p} \cdot V_{0p}}\right)^2 \cdot \left(\frac{\mu_{mp}}{\mu_{hp}}\right)^2 \cdot \left(\frac{V}{V_{0p}}\right)^{2(\beta_{1mp}-\beta_{1hp})} \cdot \left(1 - \frac{V}{V_{0p}}\right)^{2(\beta_{2mp}-\beta_{2hp})}$
- $M_Q^2 = \left(\frac{M/B}{m_{0p} \cdot V_{0p}}\right)^2$
- $N_Q^2 = \frac{2 \cdot a \cdot H \cdot M/B}{h_{0p} \cdot m_{0p} \cdot V_{0p}^2} \cdot \frac{\mu_{mp}}{\mu_{hp}} \cdot \left(\frac{V}{V_{0p}}\right)^{(\beta_{1mp}-\beta_{1hp})} \cdot \left(1 - \frac{V}{V_{0p}}\right)^{(\beta_{2mp}-\beta_{2hp})}$
- $V_Q^2 = \mu_{mp}^2 \cdot \left(\frac{V}{V_{0p}}\right)^{2\beta_{1mp}} \cdot \left(1 - \frac{V}{V_{0p}}\right)^{2\beta_{2mp}}$

All the parameters are defined analogously as for the yield surface. The additional subindex ”p” is added to separate them from the parameters characterizing the yield surface. The exception is V_{0p}, which is solved by imposing Q=0.

Chapter 4

Test facility

In this chapter the facilities for the prototype-tests are presented, as well as the planned tests. The tests are later used for validating the macro-model.

4.1 Scale model test facility

The model test facility at the Geotechnical Division, NTNU, consists of a main test chamber in concrete with an area of 4.0 x 4.0 m^2, a depth of 3 meters and an automated sand-handling facility. The maximum capacity of this chamber is approximately 80 tons, all of which is circulating the system schematized below in Figure 4.1. The test tank can be emptied and the sand transported from the conveyor belt to the bucket elevator and then to the storage silo, all during the emptying of the tank. Thereafter, the sand is transported to an automatic spreader-wagon which passes back and fourth at a speed of around 8 cm per second, dropping sand in the test tank from openings in the bottom of the spreader. The in-situ porosity can be varied by changing the 456 nozzles at the bottom of the spreader(7, 10, 16 and 20 mm are available). According to Lieng (1988) previous studies show that there is a satisfactory small variation of density from top to bottom of the test chamber.

In order to get a smooth sand surface a vacuum-cleaner is used. It is supported by the steel-frame and guided back and forth on rollers to even the sand out. The vacuum cleaner never touches the sand, but removes sand from the somewhat uneven top-layer, rendering the surface smooth.

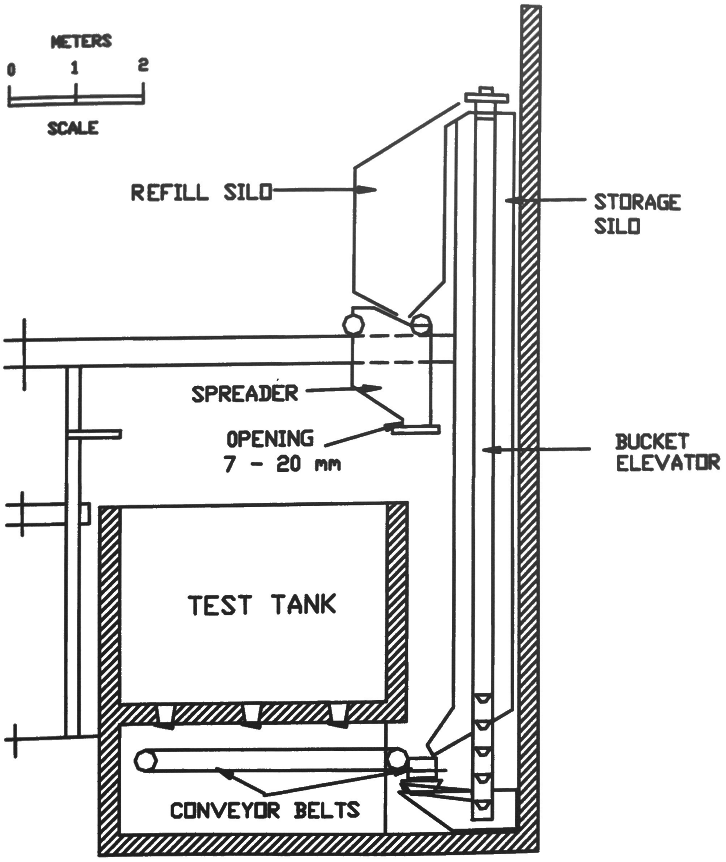

Figure 4.1: Cross section of the test tank and the sand handling equipment. Picture taken from Tefera (2004)

4.2 Scale model test set-up

As argued earlier the nature of the problem is found sufficiently described by three degrees of freedom, and the small scale-tests are done thereafter. The foundation is a steel-box, rigid with respect to the soil. The aim is to control the application of vertical-, moment- and horizontal forces and the corresponding displacements. In order to do so, there are three points of displacement-application, all of which are added through ball-screws. The ball-screws can be controlled with an accuracy of 1/250mm. Underneath the steel-box foundation sand is glued by Sikaflex-11FC. This is done so that the interface roughness between sand and the foundation should be approximately 1.

At each point of application there are hinges rendering the points free of moment. The points of application are: (i)pure vertical force applied in the centre of the foundation; (ii) a force applied 1m above the foundation base; and (iii) a force applied 0.1m above the foundation base.

By applying different magnitudes of displacement by the two forces acting 0.1 and 1m above the foundation base, a rotation can be introduced to the foundation, and thus a moment.

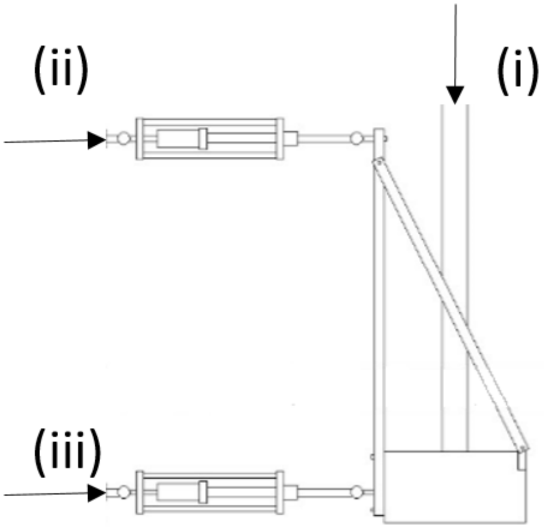

Figure 4.2: Prototype foundation

A script written with the commercial software LabView is used to control the application of either force, or displacement. Thence, the conducted tests can be programmed to have either displacement control, load control or combined controlled tests. To illustrate the application of displacement(or force) to the foundation it is referred to Figure 4.2. To further illustrate the model set-up, see Figure 4.3(a) and (b).

4.3 Test program

Gottardi et al. (1999) and others argue that so-called swipe tests allow for direct investigation of the yield surface. The procedure of such tests are as follows. First, a vertical displacement is applied, reaching a certain load or penetration. Thereafter, the vertical displacement is fixed and the footing is subject to purely applied displacements. The purely applied displacements will be either purely horizontal, or rotational movement. Such tests are therefore displacement controlled.

According to Martin (1994) the force paths which are traced during the swipe tests are tracking the boundaries of the ultimate yield surface at a given vertical penetration. Such tests can therefore be very efficient while investigating the geometry of the yield surface.

It is troublesome to apply purely moment- and vertical forces for the prototype foundations, without the occurrence of horizontal forces. It is therefore decided to focus on horizontal swipe-tests. As the foundation is subject to horizontal displacement the vertical force will then decrease, and horizontal fores increase until the load combination is at ultimate yield. Thence, the load combination should trace the maximum mobilized yield surface.

In addition to horizontal swipe-tests, the shape of the ultimate yield surface in the M/B-H plane is of interest. Earlier comparable tests are conducted by e.g. Butterfield and Gottardi (1994) who suggested the shape of the yield locus in the M/B-H plane as a tilted ellipse.

Therefore, the following tests are done:

1. Application of vertical force (dV > 0, $du = dB\theta = 0$)
2. Horizontal swipe test (du > 0, $dw = dB\theta = 0$)
3. Combined control with constant vertical force, and different displacement increments from the two ball-screws located 0.1 and 1m above the foundation base($dB\theta \neq 0$, $du \neq 0$, dV=0)

Special attention is given to the behavior in the M/B-H plane, and comparison will be done for both finite elements, the calibrated macro-model and the prototype-foundation. The table below show which displacament-combinations are applied for comparison. The displacement-increments below are assumed to cover a wide range of load-combinations, and are thus chosen.

V=1kN		V=2kN	
B·$d\theta$	du	B·$d\theta$	du
0.00884	-0.00211	0.00884	-0.00211
-0.00366	0.00806	-0.00366	0.00806
0.00114	0.001	0.00222	0,00099

Table 4.1: Different displacement increments tested in the M/B-H plane. All measurements in m.

However, extensive testing will be done with finite elements and for the prototype-foundation to determine the yield-surface in the M/B-H plane, but the combinations listed above are emphasized by comparison for the rest of the thesis.

4.4 Limitations

Throughout this thesis the only foundation-geometry investigated is one of 0.4 x 0.2 m^2. The maximum vertical force that can be applied in the test-chamber is 2.5kN. This is approximately

15% of the pure maximum vertical capacity for the geometry tested. Therefore, an extensive prototype-testing program is done with a vertical force of 1kN and 2kN in the M/B-H plane.

Gottardi and Butterfield (1995) conclude that laboratory tests under the influence of 1 g (9.81 m/s^2) cannot properly predict the behavior of large foundations, due to scale effects. However, the response of small-scale foundations are important for better understanding the upscaled in-situ behavior.

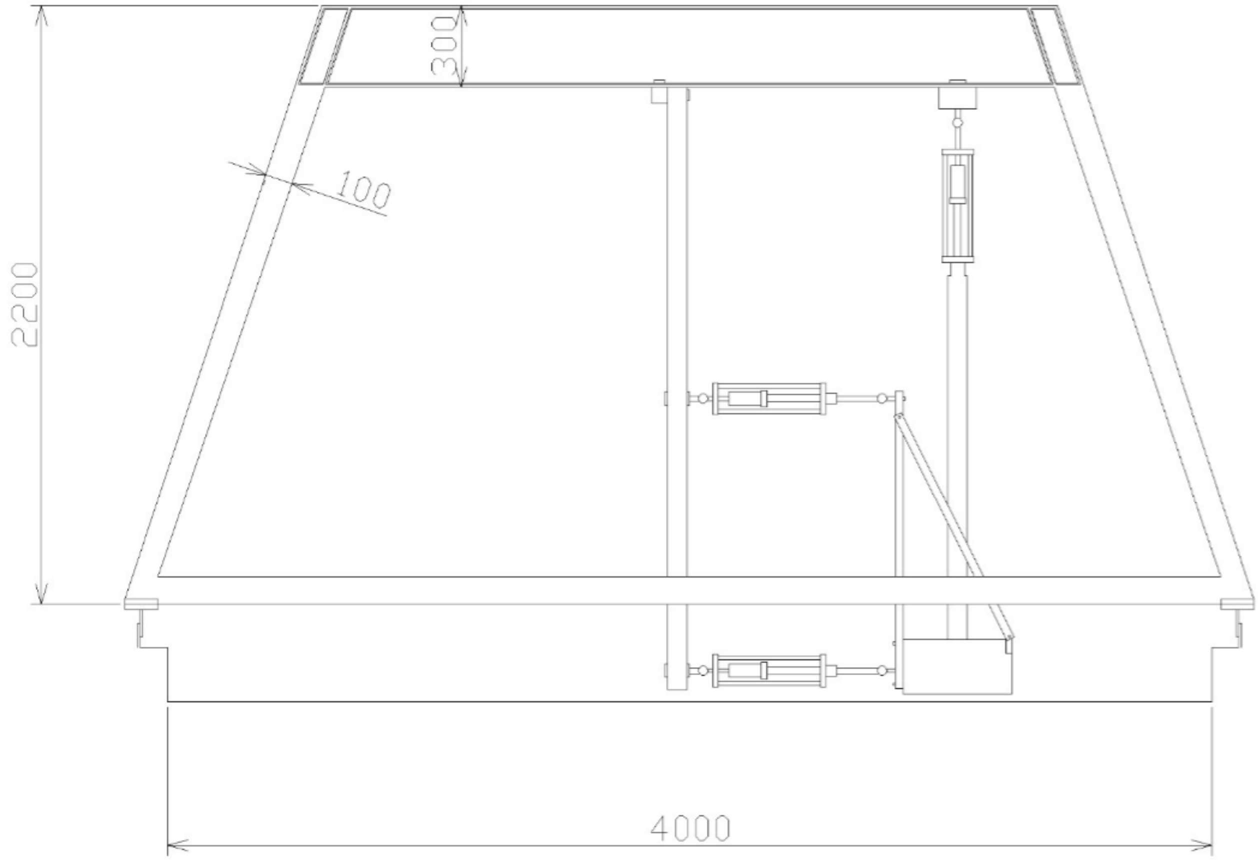

(a) Steel frame and loading equipment. All measurements are in mm.

(b) The loading cells and set-up is shown.

Figure 4.3: The prototype-foundation set-up is shown

Chapter 5

Experimental work on the model-sand

In this chapter the sand on which the prototype foundation will stand is subject to investigation. Both index-, as well as triaxial tests are done. On the basis of the conducted tests soil parameters for the Hardening Soil-model are suggested for use in the numerical analyses and calibration of the macro-model, which will be presented in Chapter 6.

5.1 General

The strength- and deformation-characteristics of a granular material is heavily dependent on how tightly packed the grains are. Thus, the macro-behaviour of the material is strongly dependent on the micro-structure. The micro-structure can be described by the grain shapes, the degree of compaction, the grain size, mineralogy and grain uniformity. Because sand loses its structure once it is removed from the sand-bin, the in-situ porosity is important when reconstructing the material structure for triaxial testing. Several laboratory tests are done. Each laboratory test is done at least three times, and the presented results of the index tests are average values. See Appendix A if the results of a particular laboratory test is of interest.

The investigated sand consist of two thirds of so-called Hokksund-sand, whilst the remaining part is so-called Sponesand. Both are natural glacifluvial deposits. In the following are several tests on the model sand.

5.2 Index tests

5.2.1 Grain size distribution

The grain size distribution of the material has been found by dry sieving according to procedures described ISO 17892-4:2016, and is shown in Figure 5.1. For comparison, previously tested Hokksund-sand and recently tested Sponesand are added.

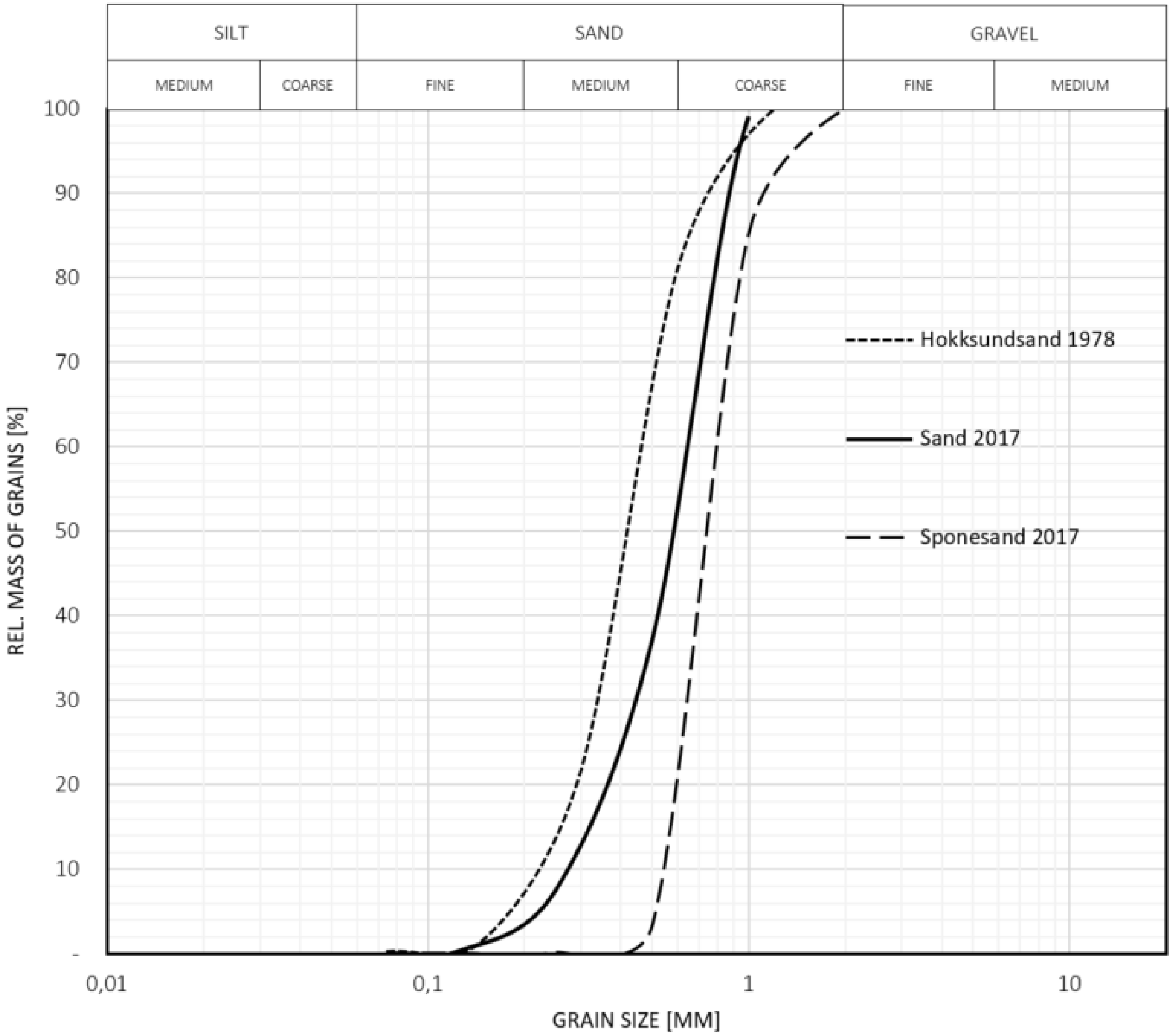

Figure 5.1: Comparison with previous grain size distributions

5.2.2 Mineralogy

Mineralogy tests have been done previously for the Hokksund-sand, and Sponesand. Both these results are added below for comparison.

Table 5.1: Mineralogy for the Hokksund-sand, by Sandven (1992).

Mineral	[%]
Quartz	35
Al	25
K-feldspar	20
Mica	10
Amphibole	5
Others	5

Table 5.2: Mineralogy for the Sponesand, provided by Sibelco Nordic.

Mineral	[%]
Quartz	84
aluminum oxide	8
Others	8

The 2:1 combination of these two lead the soil to be defined as quartz-sand ($S_I O_2$).

5.2.3 Grain density

The grain density of the material is found by using a pycnometer and the standard-procedure outlined in ISO 17892-3:2004 is followed. The suggested value found is $2.64 g/cm^3$.

5.2.4 Water content

The sand is characterized as dry, as the water content is negligible(w=0.07%).

5.2.5 Determination of the porosity limits

The porosity limits are found in accordance with the procedures first described by DEGEBO(Deutsche Gesellschaft für Bodenmechanik), which are summarized in the following.

In order to obtain the loosest state of compaction, dry sand is led through a funnel which is slowly guided upwards. There should be a negligible fall height from the mouth of the funnel to the sand in the cylinder(A=61,5 cm^2). The equipment is shown in Figure 5.2(b). The maximum porosity is approximated as $n_{max} = 46.4\%$ and the minmum dry density 13.9 kN/m^3.

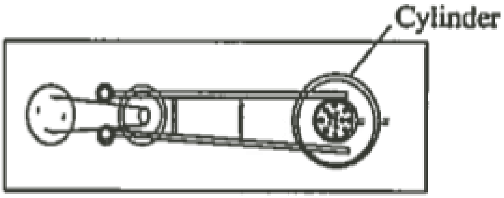

(a) The equipment for determination of the minimum porosity

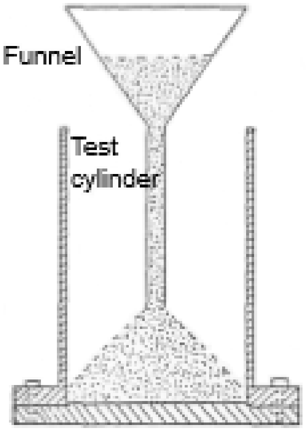

(b) The equipment for determination of the maximum porosity

Figure 5.2: Porosity limits

In order to compact the sand to its densest state the machine in Figure 5.2(a) is used. The sand is compacted in a steel cylinder(A=78.5 cm^2), with four resulting layers of sand, each with a height of approximately 2 cm . Each layer of saturated sand is compacted by vibration, caused by two rods hitting the exterior of the cylinder wall for 30 seconds, after which the excess surface water is removed. The sample is then dried at what is considered its densest state and the minimum porosity suggested is $n_{min} = 35.4\%$ and maximum dry density 16.8 kN/m^3.

The relationship between the maximum and minimum porosity and the corresponding dry densities give way to the figure below. Such a figure can be useful if the dry in-situ density is known, as the relation in the figure give way to the corresponding in-situ porosity, and thus the in-situ relative density.

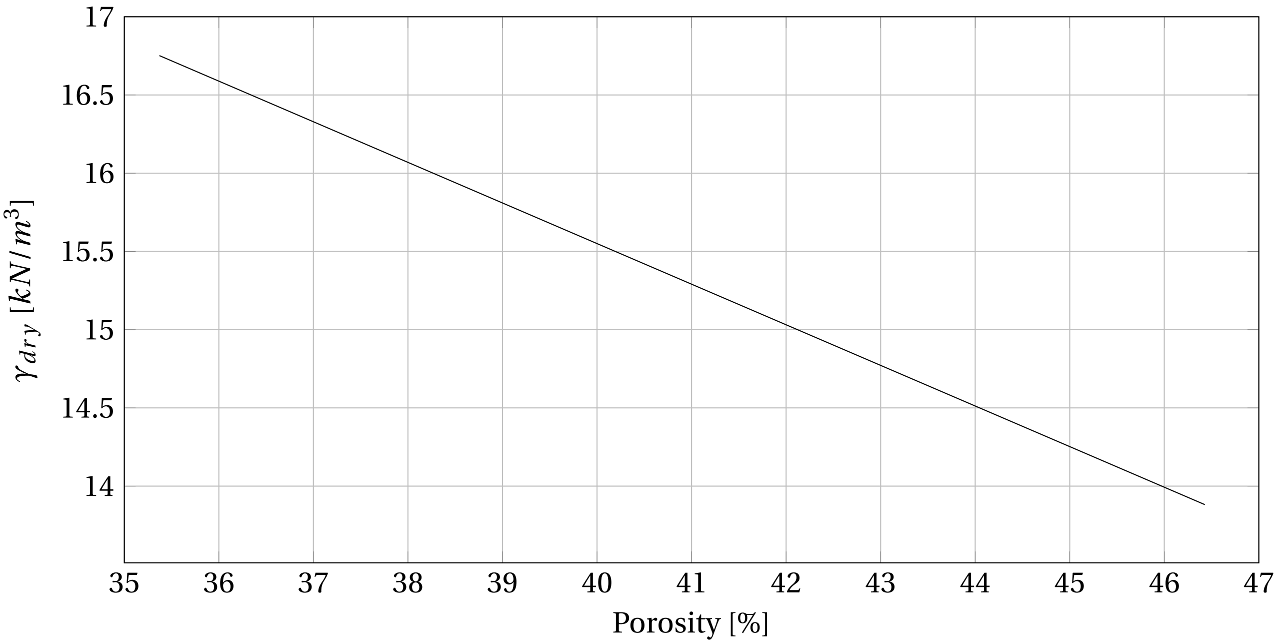

Figure 5.3: Relationship between porosity and dry density

By placing a cylindrical box with a known volume in the test chamber(see Figure 4.1) and then letting the aforementioned spread wagon sediment sand in the test chamber(including the cylindrical box) then the dry weight of sand can be measured. The dry density is found, and thus the in-situ porosity. The average in-situ density measured is $\gamma_{dry} = 15.75 kN/m^3$ and the in-situ porosity is approximated to $n = 1 - \frac{\gamma_d}{\gamma_s} = 39\%$, which means that the relative density is around $D_r = 1 - \frac{n - n_{min}}{n_{max} - n_{min}} = 65\%$. The sand is therefore characterized as one of medium porosity. The nozzle openings on the wagon spreader are set so the relative density of the sand should be 75 %, so the values obtained seem reasonable.

5.3 Triaxial tests

Triaxial tests can be very useful in order to determine the strength and stiffness of a soil. In the following are the preparation, execution and interpretation of the triaxial tests presented.

5.3.1 Preparation for triaxial testing

There are several ways of approaching the issue of preparing the sand for triaxial testing. One is known as the moist tamping technique. Yang et al. (2008) conclude that samples prepared by moist tamping can be reasonable assumed to be transversely isotropic. Due to its repeatability and simplicity it is chosen as the preferred method of sample reconstruction.

By adding some water to the sand before preparing it in the preparation mould, small meniscus forces between the grains result in some inter-granular cohesion for the sample. Thence, the sample can stand on its own after removal of mentioned mould, as seen in Figure 5.4(b). Therefore, sand with a water content of around 6%(could also be less) is put in the mould and compacted in approximately 5 layers of 2 cm. Each layer should be subject to the same amount of energy in order to obtain homogeneity. The degree of compaction is heavily dependent on the amount of tamps for each layer and the height of the fall height of the tamping rod. Therefore, obtaining the in-situ compaction requires some trial and error, before realizing how many tamps are necessary to acquire the in-situ dry density.

To obtain a relative density of approximately 65%(in-situ relative density) the following routine was found quite effective. The first layer is subject to 5 tamps and then the amount of tamps is increased by 5 for each layer. The fall height of the tamping rod is 1 cm, and it is assumed that with such a small fall height grain crushing whilst preparing the sample is considered unlikely.

After the sand is compacted to the desired porosity the mould is removed, the triaxial cell is placed around the sample and the cell filled with water. See Figure 5.4.

Introductory analysis with finite elements shows that during loading the prototype foundation will experience minimum principal stresses in the soil close to the foundation in the range between 6-40 kPa for the planned load-combinations in the sand-bin. Therefore, the aim of the test program is to find the strength and stiffnesses at what is considered representative confining stress ranges.

5.3.2 Triaxial tests on model-sand

The degree of saturation before the consolidation phase of the triaxial is unknown. After the consolidation phase the sample will be saturated, but how the sample volume has changed is not known. The change in volume of the cell is not measurable with the triaxial apparatus used during consolidation, and one can only make assumptions. One assumption is $\varepsilon_{vol} = 2.5 \cdot \varepsilon_a$, which would lead to a slight decrease of the volume, and thus to the porosity. Such an assumption leads to maximum 0.1 % change in porosity for all tests done. During consolidation the pore pressure decrease is relatively small(around 10% for all tests), which may indicate that the samples are already having a degree of saturation relatively close to unity. The porosity is therefore assumed to the same after consolidation as before.

In the following are the most successful of the in total 18 compression triaxial tests done. All are consolidated isotropically and drained tests with confining pressures ranging from 20 to 40 kPa. The soil behavior is highly dependent on the compaction of the sample, and as mentioned

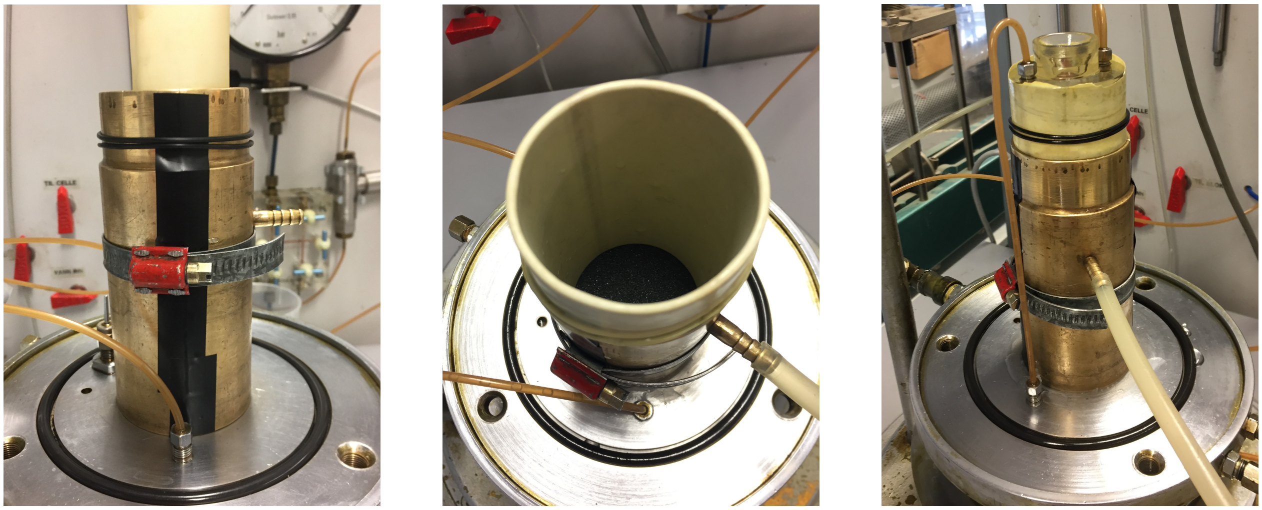

(a) The mould is put on the triaxial pedestal and the sand is built in as previously explained.

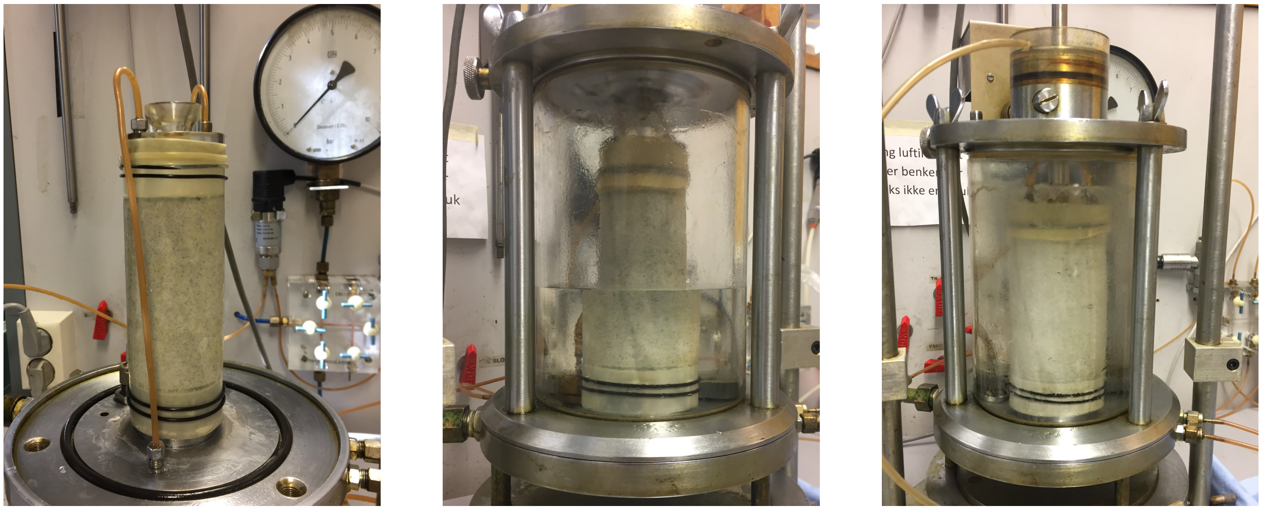

(b) The mould is removed, and the cell is placed around the sample.

Figure 5.4: Build-in process of the sand

earlier the in-situ relative density was approximated to 65%, which leaves the test of 20kPa closest to the in-situ compaction, while the one with 40 kPa too dense and the one of 30 kPa too loose. However, as will be apparent the soil response is quite similar for the three samples presented. One of the parameters necessary for the Hardening Soil-model presented in Chapter 3 is the unloading-reloading stiffness, which is why an unloading-reloading loop can be seen in all the following triaxial tests.

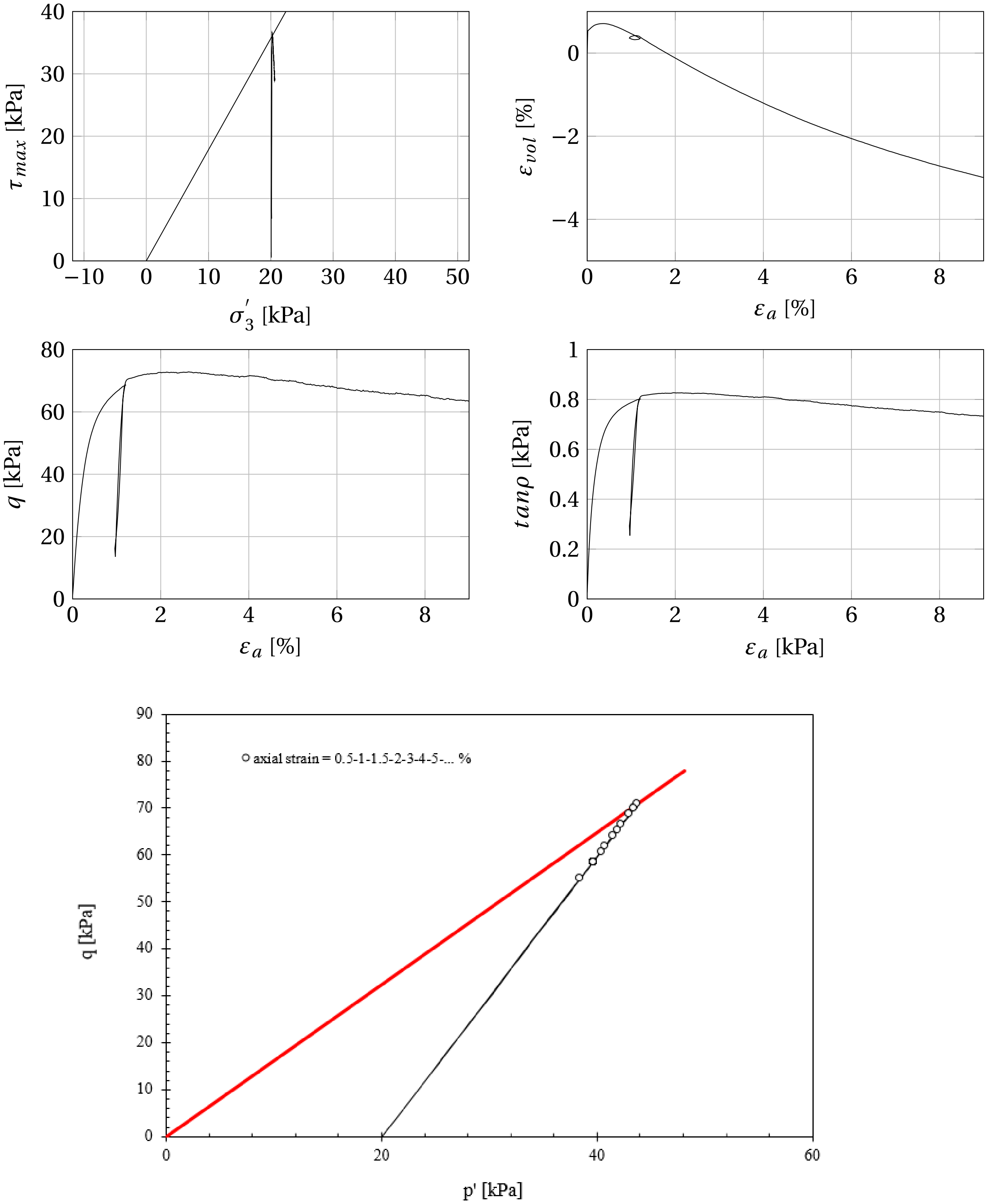

Figure 5.5: Triaxial test with a confining pressure of 20 kPa and relative density of 66.7%

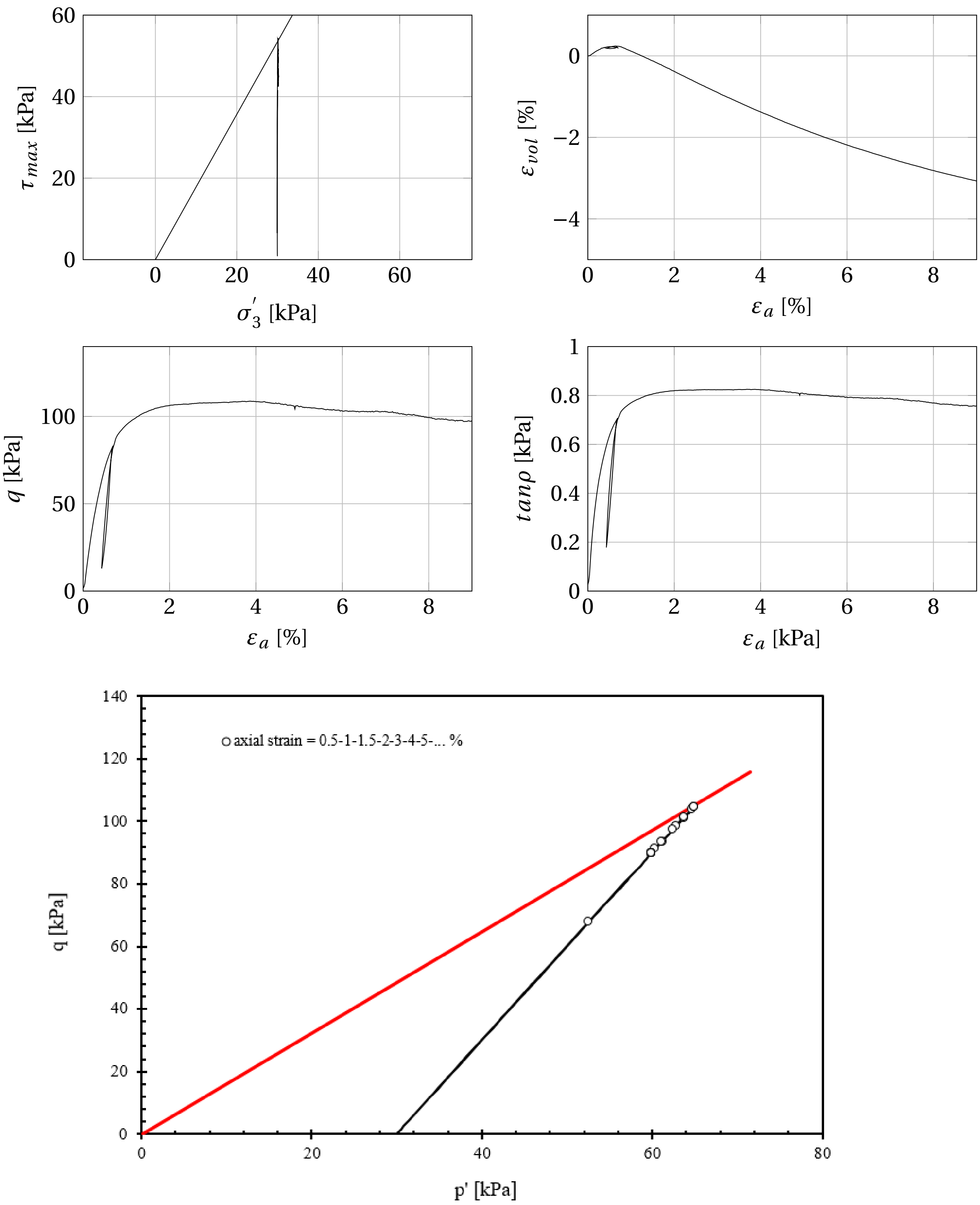

Figure 5.6: Triaxial test with a confining pressure of 30 kPa and relativedensity of 59.1%

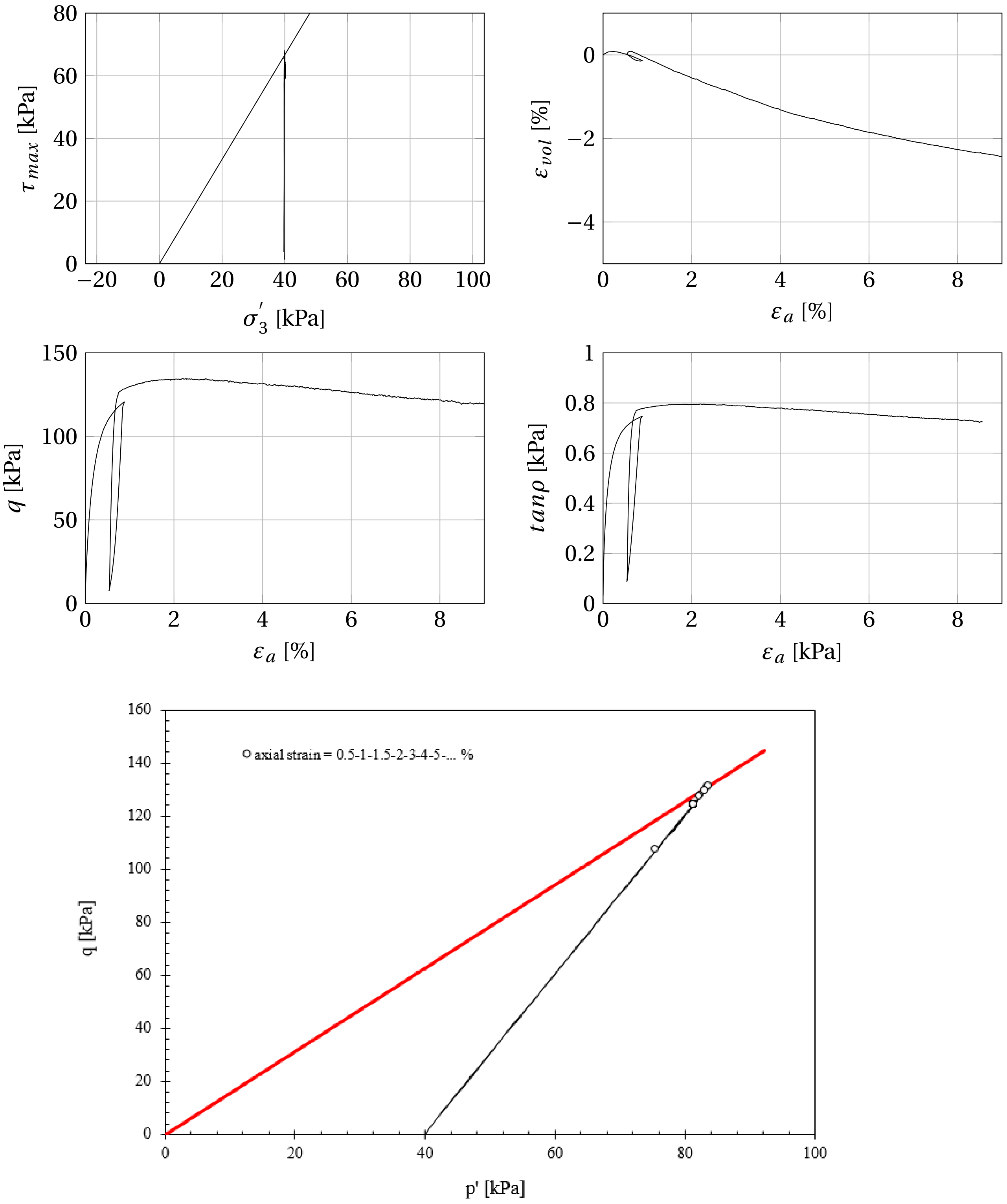

Figure 5.7: Triaxial test with a confining pressure of 40 kPa and relative density of 72.8%

5.3.3 Triaxial test interpretation

From the triaxial test with 40kPa in confining pressure the unloading-reloading loop does not seem to be as linear as the other tests. This is because the triaxial program is run with a step motor, data is saved every so often and the deformation during the unloading-reloading loop had higher increments than the other two tests. The stresses in this range are deemed trustworthy, but the axial strain seems to be slightly off. Therefore, the triaxial tests with a confining pressure of 20 and 30 kPa are investigated when choosing a representative set of Hardening Soil-parameters. The General Soil-Test option in Plaxis, version 2016.01, is used.

Some assumptions are made, e.g. that the oedometer stiffness is the same as the secant stiffness E_{50}, as no oedometer tests were done. This is a reasonable assumption as pointed out by e.g. Nordal (2016). The dilatancy cut-off parameters are chosen on the basis of the contractive, and then dilative behavior observed in the triaxial tests. e_{max} prevents the soil to theoretical infinite dilation, and by setting this value to 0.71, while $e_{init} = 0.645$, the maximum volumetric change is limited at $e_{vol} = 4\%$ as seems to be the case on the basis of the representative triaxial tests done. The e_{min} controls the maximum volumetric contraction during shear, but it is not essential, as the material quickly starts to dilate after an initial contraction in the shear-phase.

The cohesion is assumed negligible, but is set to 0.1kPa to avoid potential numerical issues (which is not a problem for the newest versions of Plaxis, but could be troublesome for earlier versions). The modulus exponent m is set to 0.4 as the curves for both 20 and 30 kPa confining pressure corresponds well with this value. These triaxial tests are compared with one set of parameters in Soil-Test and presented in Figure 5.8 and 5.9. The associated Hardening Soil-parameters are given in Table 5.4.

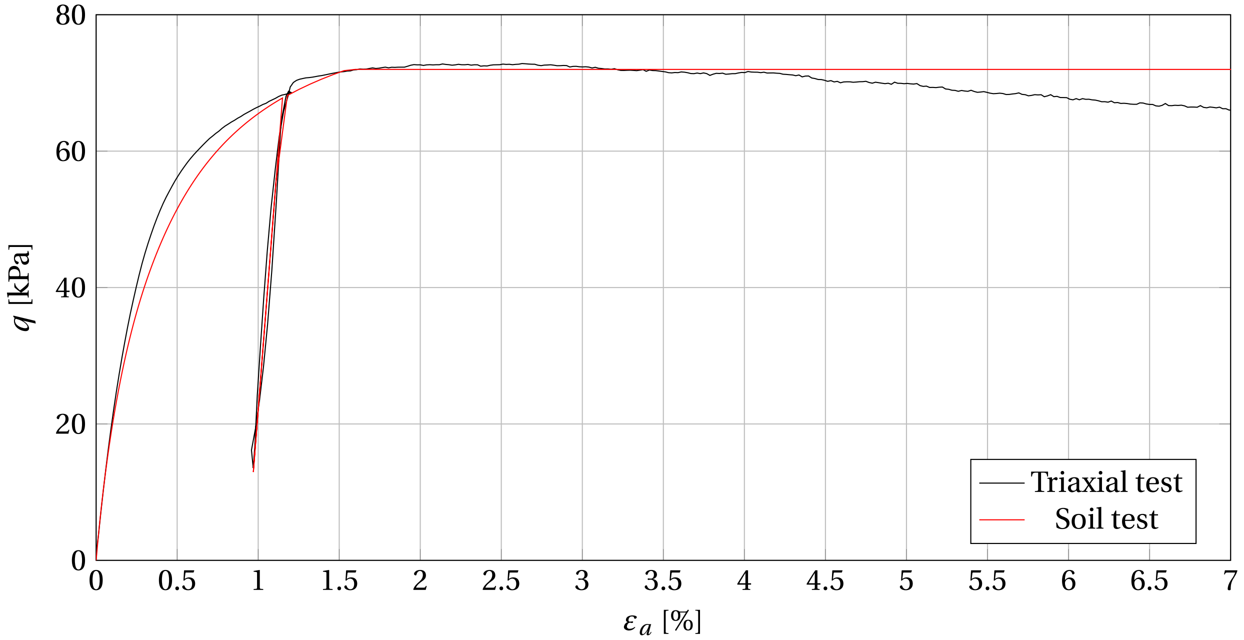

Figure 5.8: Triaxial- and Soil test with a relative density of 67% and confining pressure 20 kPa

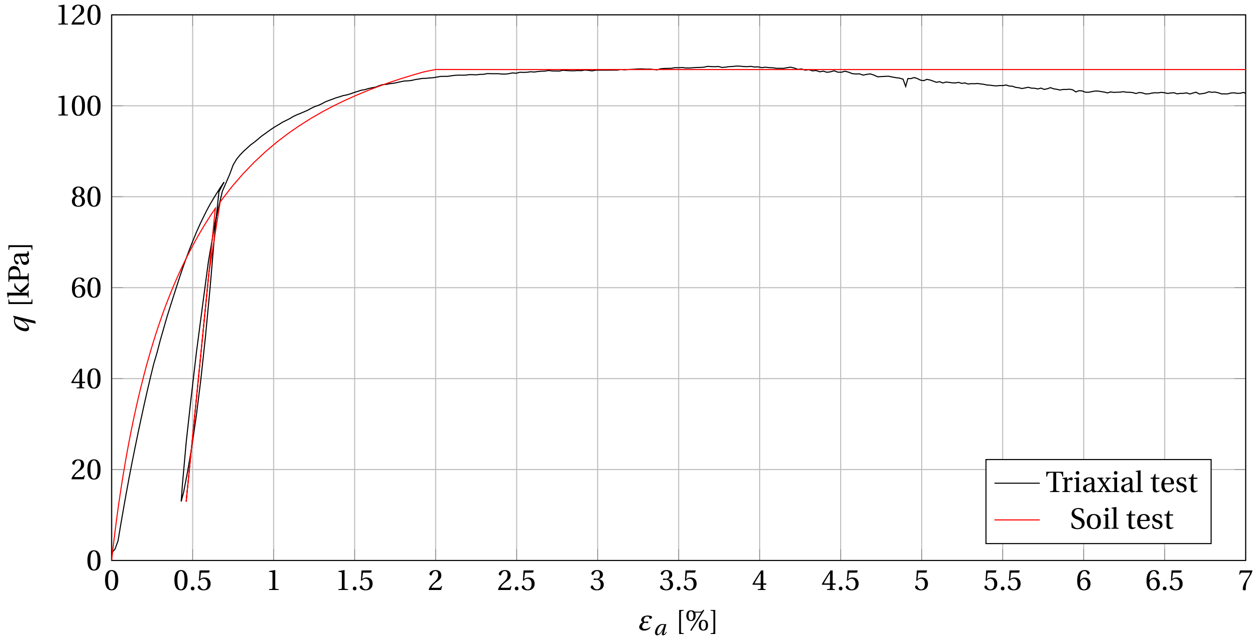

Figure 5.9: Triaxial- and Soil test with a relative density of 59% and confining pressure 30 kPa

5.4 Summary of the soil characteristics

The model-sand investigated is characterized as a uniform, medium grained and medium dense quartz-sand. The two following tables summarize the conducted laboratory-tests.

Parameter	Value
$C_u = d_{60}/d_{10}$	2.3
d_{50}	0.6 mm
ρ_s	2.64 g/cm^3
w	0
n_{max}	46.4%
n_{min}	35.4%
D_r	65 %

Table 5.3: Index test summary

Parameter	Value
E_{50}^{ref}	28MPa
E_{oed}^{ref}	28MPa
E_{ur}^{ref}	58MPa
m	0.4
Rf	0.85
OCR	1
$K_0^{nc} = K_0$	1-sinϕ=0.36
φ	39.5 °
ψ	11.5 °
c	0.1 kPa
υ_{ur}	0.2
e_{init}	0.645
e_{max}	0.71
p_{ref}	100kPa

Table 5.4: Hardening Soil parameters summary

Chapter 6

Calibration of the macro-model

By simulating the application of different load-combinations, the capacity and soil behavior are investigated by finite elements. On the basis of the obtained results, the 24 necessary parameters for the macro-model are chosen.

The macro-model is run with a script coded in MATLAB, version R2016a. The script can be either run with displacement-, load- or combined control. Thence, the first step of calibrating the macro-model is ensuring adequate match with the compared results obtained in Plaxis.

6.1 Introductory analysis

The chosen finite-element software is Plaxis 2D, version 2016.01, run with 15-noded triangular elements in plane strain conditions.

6.1.1 Choice of mesh and pure vertical capacity

The first finite element analysis(FEA) done is an investigation into the maximum vertical bearing capacity. The chosen mesh is the coarsest one, where no further refinement leads to a change of vertical bearing capacity. The refinement was first and foremost done locally close to the foundation. The mesh used is shown in the figure below.

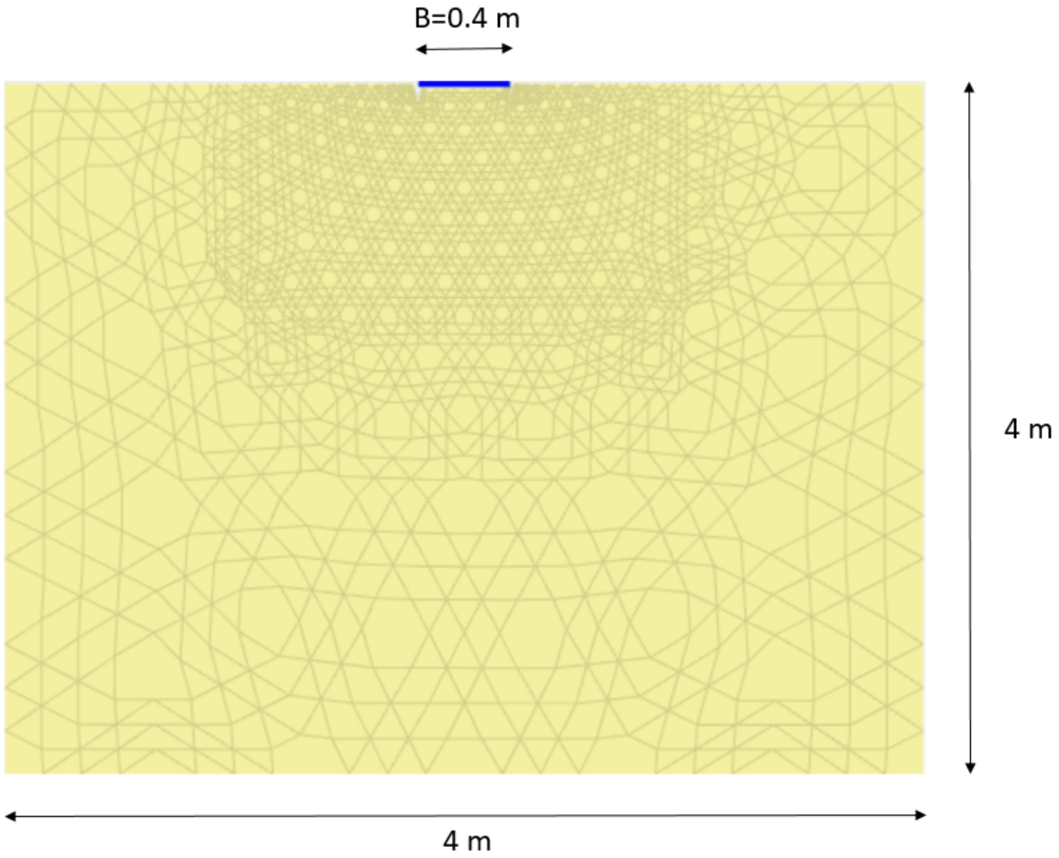

Figure 6.1: Chosen mesh for the finite element analysis

As can be seen from Figure 6.2 the ultimate bearing capacity is not uniquely defined at a singular load, but rather oscillating. This can be attributed to the non-associativity of the problem, and that Plaxis has difficulties in deciding on which mechanism is more critical. However, for the finer mesh a maximum vertical bearing capacity is set at 14.5kN. A further refinement of the mesh does not lead to a change in bearing capacity.

This ultimate bearing capacity is high compared to the expressions proposed by e.g. Terzaghi(11.5kN, according to Equation 3.1), Brinch-Hansen(10.4kN, according to Equation 3.2) and Janbu(11.6kN, according to Equation 3.3).

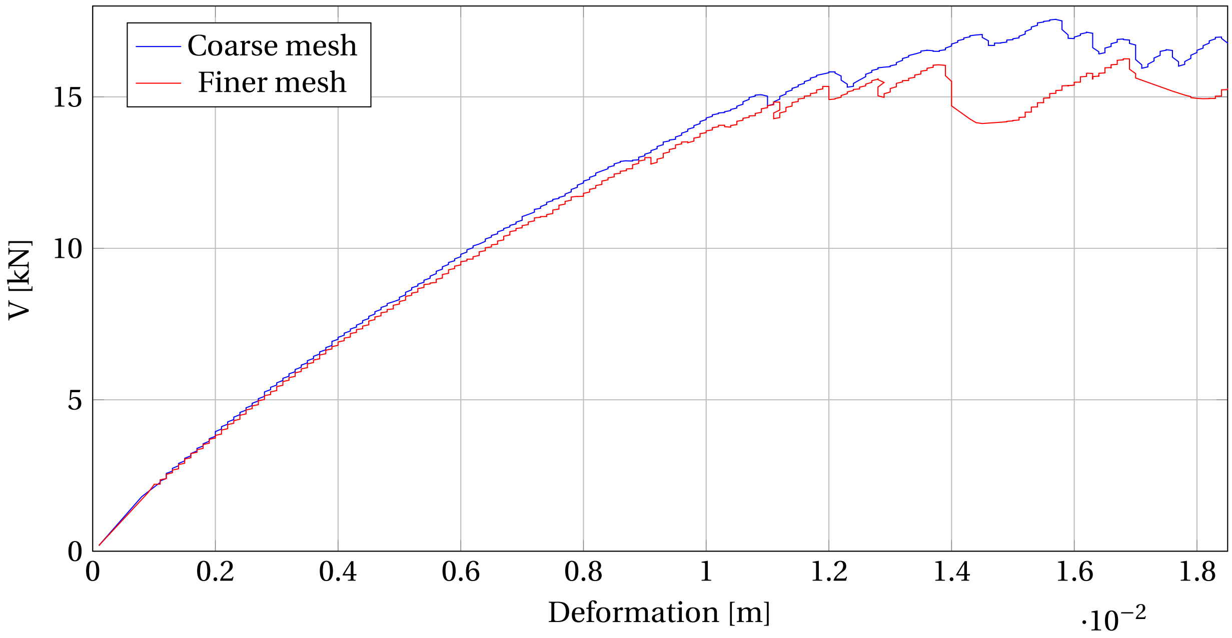

Figure 6.2: Vertical bearing capacity versus deformation

6.2 Yield surface

The calibration of the yield surface is done through swipe-tests in the V-H and V-M/B planes, as well as observation of the behavior in the M/B-H plane.

6.2.1 M/B-H plane and ”a”-factor

To observe the behavior in the M/B-H plane the vertical load is held constant, while rotational and horizontal displacement increments are imposed on the foundation. The model used in Plaxis to achieve this end is shown in the figure below, and two phases are applied:

1. V=1 kN
2. dV=0. du and $Bd\theta$ are applied from point displacements points 0.1m and 1m above foundation base to simulate the prototype-tests

With different magnitudes of the two point displacements the foundation is subject to rotation. The size of the imposed rotation depends naturally on the difference between the two point displacements applied.

The formula proposed by Butterfield and Gottardi (1994) is used to account for the ellipse-rotation:

$$a = tan2\rho \cdot (t_h - t_m)(t_h + t_m)/2t_h t_m \tag{6.1}$$

The t_h- and t_m-values are the initial slopes of the yield-locus in the V-H- and V-M-planes.

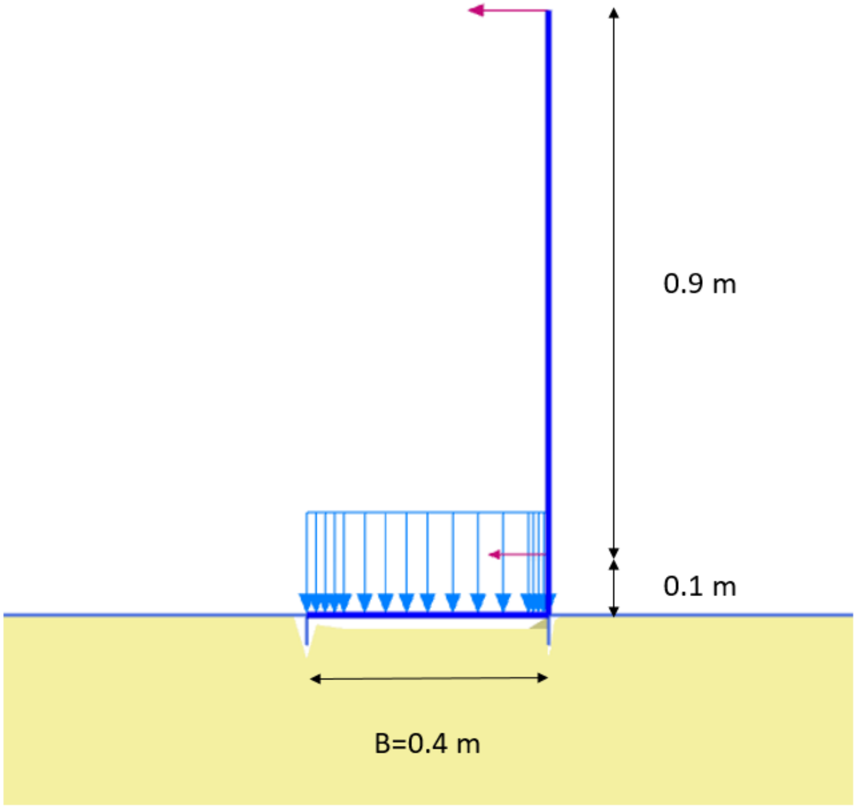

Figure 6.3: Plaxis model for the M/B-H tests

Thence, force paths can be traced to ultimate yield. The points in the following figure indicate failure, and on the basis of these points an ellipse is suggested as a generalized shape in the M/B-H plane. The plane investigated is that of 1kN. There is suggested a rotated ellipse on the basis of the observed failures. The rotation in Figure 6.6 is rotated 6 degrees and has an axis ratio of 1.61.

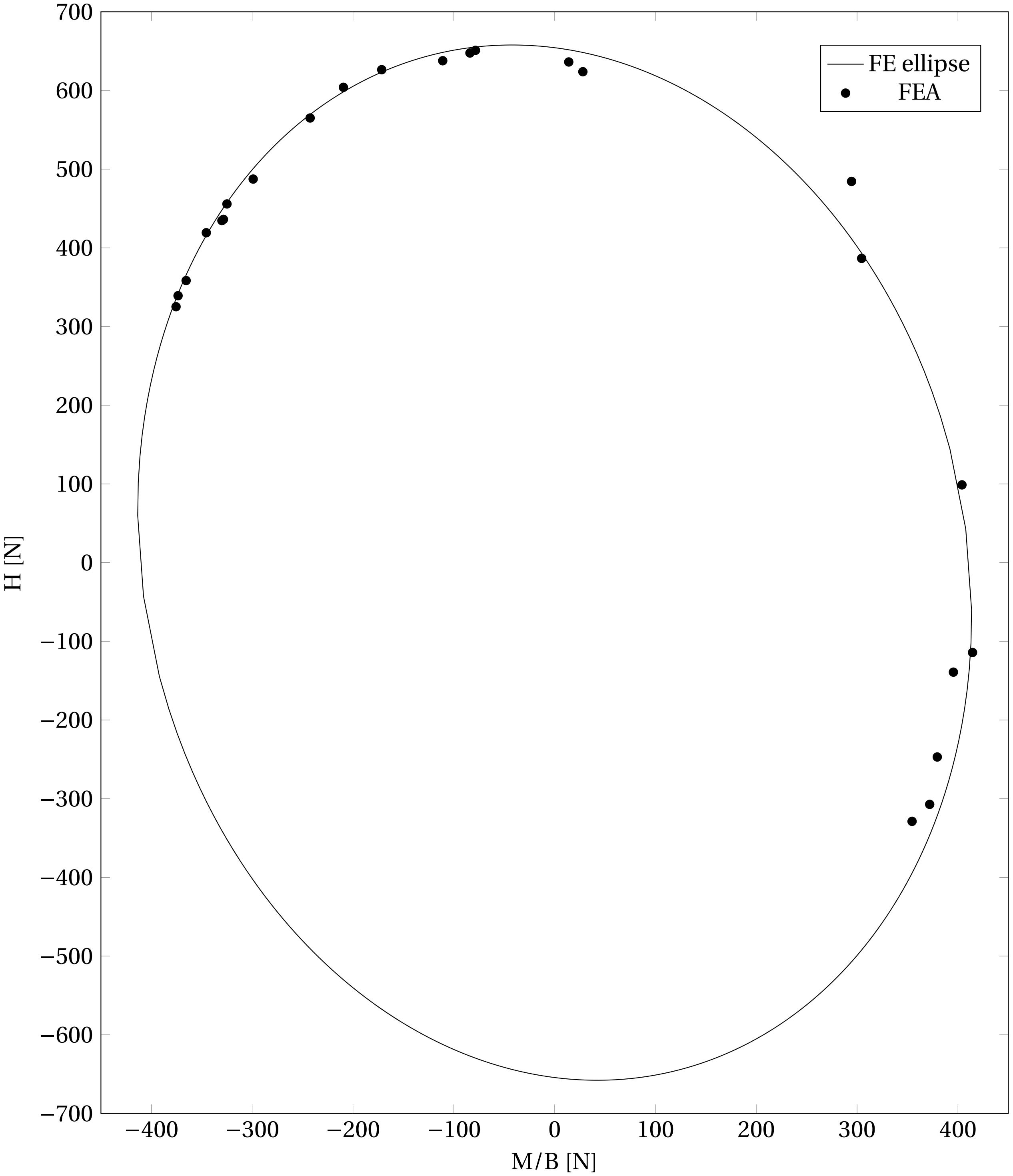

Figure 6.4: M/B-H plane for V=1kN

6.2.2 Swipe

The concept of swipe testing is outlined in Chapter 5.3. The β-values control if the loci are leaned towards V_{max}, or zero vertical force, and to which extent. The h_0 and m_0 values are chosen for an appropriate maximum horizontal and moment-loading. This is modelled simply by having an initial phase of vertical load application, and then a second phase of either pure horizontal or rotational movement (the vertical displacement is fixed).

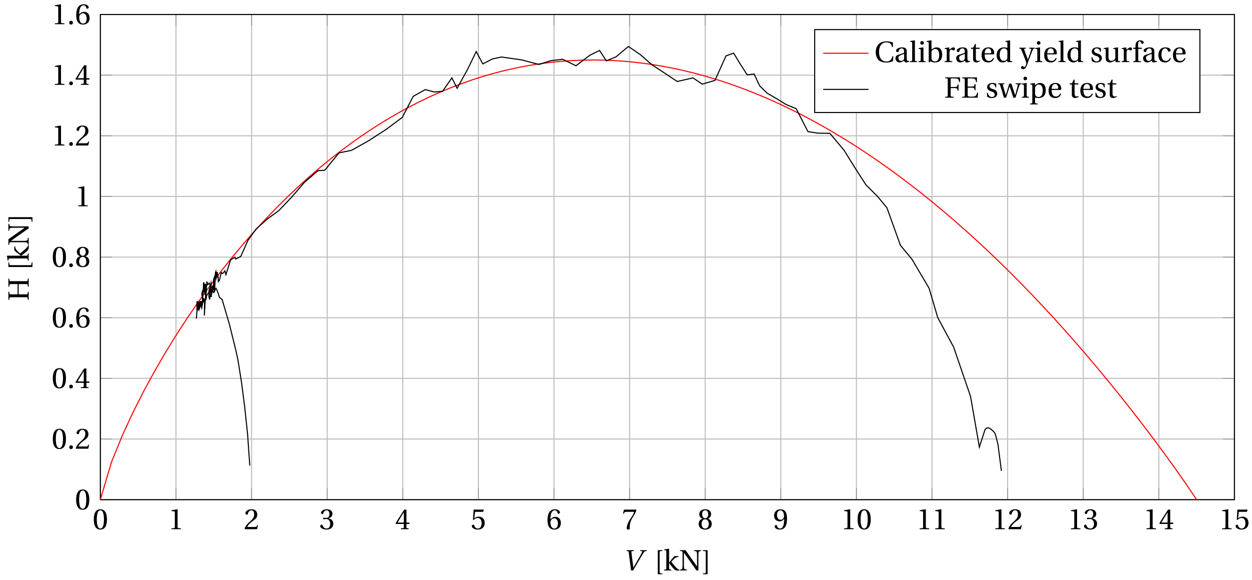

Figure 6.5: Horizontal swipe test

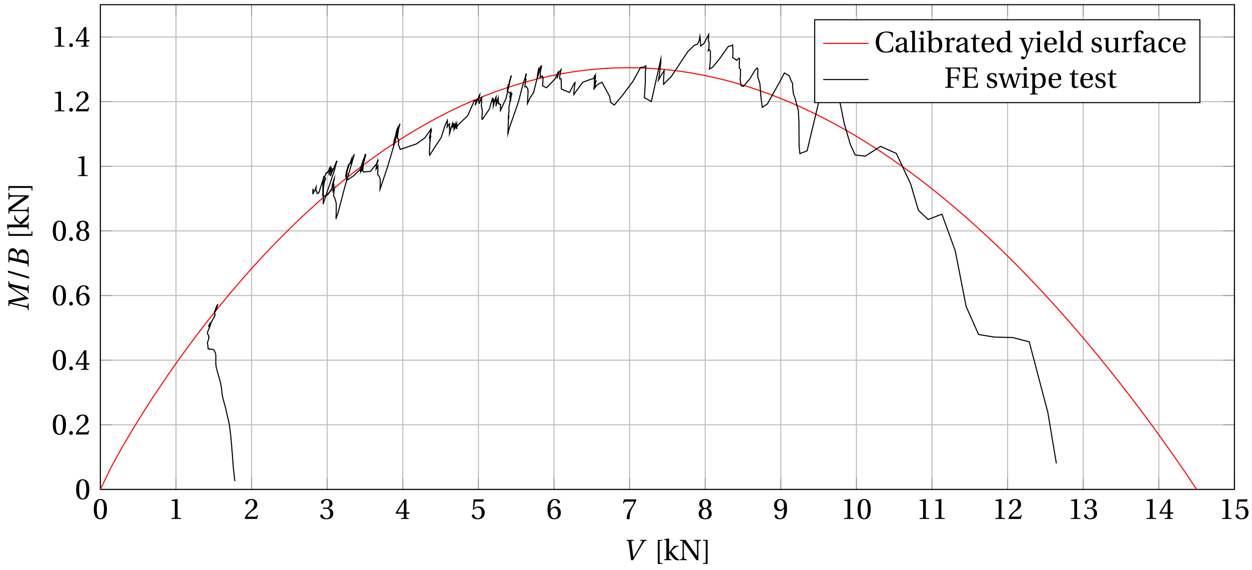

Figure 6.6: Swipe test in the V-M/B plane

6.3 Elastic behavior

As already discussed in Section 3.4.4, the dimensionless diagonal stiffnesses of the matrix can be determined from the semi-analytical relations given by e.g. Pais and Kausel (1988).

For comparison the same same static stiffness terms as found by Gazetas (1991), Dominguez(1978) and Wong and Luco(1978) are added in Table 6.1, with the ratio L/B being 2 and Poisson' ratio 1/3.

	Gazetas	Dominguez	Wong and Luco	Pais and Kausel
k_1 [-]	2.469	2.625	2.524	2.555
k_2 [-]	0.490	0.459	0.474	0.468
k_3 [-]	1.912	1.965	1.943	1.961

Table 6.1: Comparison between stiffnesses for L/B=2 and $v = 1/3$

The stiffness values are similar, and as Pais and Kausel formulated their expressions based on the work done by the other authors named in the table, the stiffnesses of Pais and Kausel are used. The k_4 values are approximately two orders of magnitude lower than k_1,k_2 and k_3 and thus neglected.

When choosing an elastic shear modulus one needs first to decide at which depth, and thus which stress, a representative shear modulus G can be found. By either turning to theory describing plastic shear zone-geometry for the foundation-geometry(B=0.4m), or by observing shear zone-geometry with finite-elements at failure it is apparent that a representative depth of G should be around a depth of 0.2-0.3m below the surface. With a soil unit weight of approximately $16kN/m^3$ and a typical vertical load of 1.5kN the stress at which G should be representative is around 8 kPa. This suggested by assuming a $K_0^{'}$ of 0.36 ($K_0^{nc} = 1 - sin\phi$), and further arguing that the minimum principal stress is assumed to be approximately K_0^{nc}(γ_{dry}·representative depth+$\frac{V}{area}$)=0.36($15.8kN/m^3 \cdot 0.25m + \frac{1.5kN}{0.2 \cdot 0.4m^2} = 8kPa$.

With reference to the triaxial test with a cell-pressure of 20kPa and a correct in-situ density the initial Youngs' modulus is 22MPa. It is assumed that this value is representative also for confining pressures lower than 20kPa. By further assuming an elastic isotropic material this leads to a shear modulus of 8.3MPa.

6.4 Hardening parameters

The plastic displacements must be related to the degree of mobilization, which for the macro-model is described only by one state parameter, namely κ. As outlined in Chapter 3.4.5 the dependence of the vertical plastic displacement is clear, whilst the importance of each contribution of the remaining plastic displacements are determined by constants C_1 and C_2. Therefore, it is found convenient to stay in the M/B- H plane by combined controlled tests. This is done as previously explained in Section 6.2.1.

Thence, the load-paths are traced towards ultimate failure, and through observation of the incremental load and displacement-vector for each step the calibration of representative hardening-parameters can be done. This is done as follows. The total displacements and forces from the FEA are extracted. By definition the total displacement is $d\boldsymbol{v}^{tot} = d\boldsymbol{v}^{e} + d\boldsymbol{v}^{p}$, and this in turn leads to the following incremental plastic displacements:

$$\begin{bmatrix} dw^p \\ B\theta^p \\ du^p \end{bmatrix} = \begin{bmatrix} dw^{tot} \\ B\theta^{tot} \\ du^{tot} \end{bmatrix} - \frac{1}{GB} \begin{bmatrix} 1/k_1 & 0 & 0 \\ 0 & 1/k_2 & 0 \\ 0 & 0 & 1/k_3 \end{bmatrix} \begin{bmatrix} dV \\ dM/B \\ dH \end{bmatrix} \tag{6.2}$$

The hardening law is chosen by curve-fitting the to the FEA results. When the incremental plastic displacements are extracted from the FEA, the combined plastic displacement can be defined from Equation 3.17. Thence, the curve for combined plastic increments from the FEA is evaluated. Then there should be sufficient fit with the chosen hardening law formulation.

However, the evolution of combined plastic displacement U_p is heavily dependent on the load-combination, and thus the ratio between H and M/B. It is important to define what is a representative ratio for the loads acting on such a foundation. As can be seen from the figure below(H/M/B)=1.15) the bi-linear relationship as described in Equation 3.18 corresponds well.

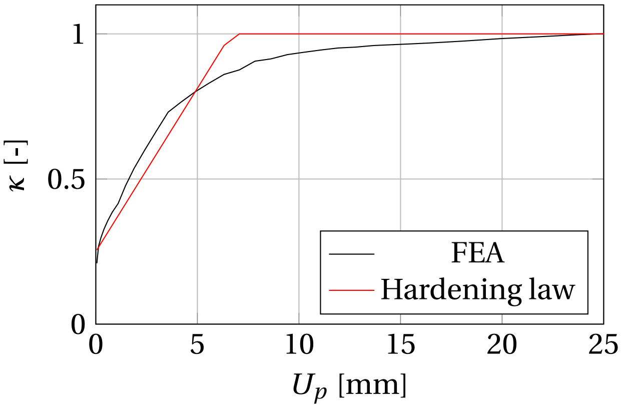

Figure 6.7: State parameter vs combined plastic displacement for H/(M/B)=1.15

6.5 Potential surface

Plastic increments develop when the material yields, and are directed orthogonal outward of the potential surface. The potential surface therefore defines the direction of plastic flow, as well as being an ingredient when deciding the size of the plastic multiplier dλ. In this thesis the parameters defining the potential surface are chosen by curve-fitting the macro-model behavior to the behavior observed from the FEA.

Extra attention is given to the macro-model's capacity to reproduce uplift behavior. It is of utmost importance for a shallow surface foundation anchoring large eccentric forces. Uplift of the foundation-centre happens when the effective width is half of the total width. The relationship between effective and total width for an eccentric load becomes:

$$\frac{B_{effective}}{B} = \frac{B-2e}{B} = 1-2\cdot\frac{M/B}{V} = 0.5 \tag{6.3}$$

Therefore, the foundation should experience positive, i.e. downward, vertical increments when M/B<0.25V. Whenever M/B≥ 0.25V the vertical increments should be negative, i.e. directed upwards. Low β_{1hp}-and β_{1mp}-values make the peak of the potential surface lean towards lower vertical loads in the V-H and V-M/B planes. Hence, the gradient is directed in a negative w-direction, for low vertical loads. This accommodates for uplift-behavior when the moment is large. How low they should be is decided by curve-fitting the FEA-results with the macro-model.

6.6 Comparison between the FEA and the macro-model

In the following the comparison between the calibrated macro-model and the results from the FEA in the M/B- H plane. The procedure is as described in Chapter 6.4 and summarized as:

1. Apply vertical force V, either 1 kN or 2 kN
2. Apply horizontal and rotational displacements du and $B\cdot d\theta$, while dV=0

As the combinations of incremental displacements are different, the force path which are traced as a result will also be different from one another. Table 4.1 summarizes the displacement-increments which will be compared with finite elements, the macro-model and the prototype-tests.

As was mentioned earlier, it is especially important for a bridge foundation that the model allows for the correct kinematic behavior regarding uplift. It was reasoned that $dw < 0$ occurs when $M/B \geqslant 0.25V$. As can be seen from Figure (V=1kN, M/B vs w) this behavior is observed

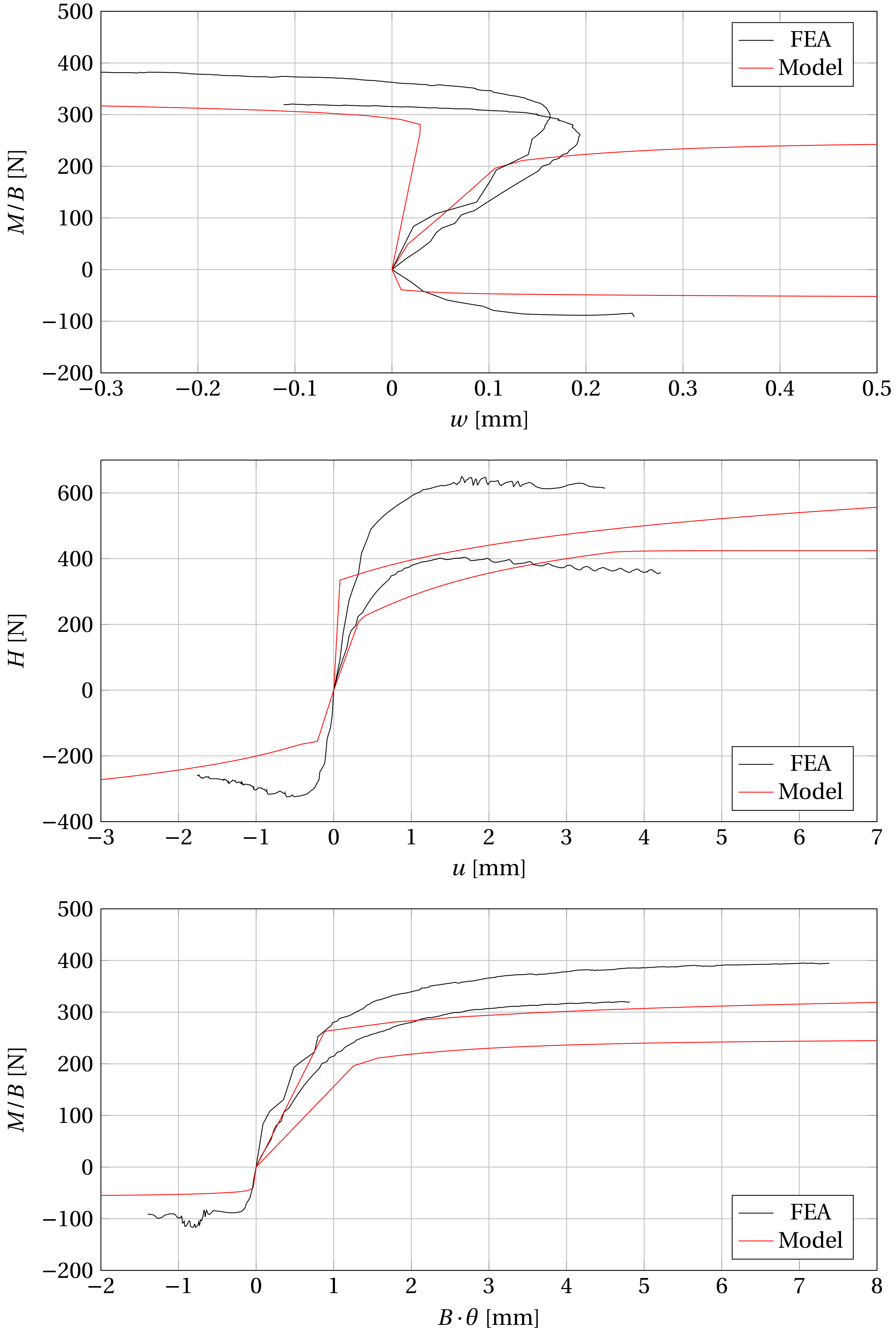

Figure 6.8: Comparison between FEA and the macro-model at V=1kN

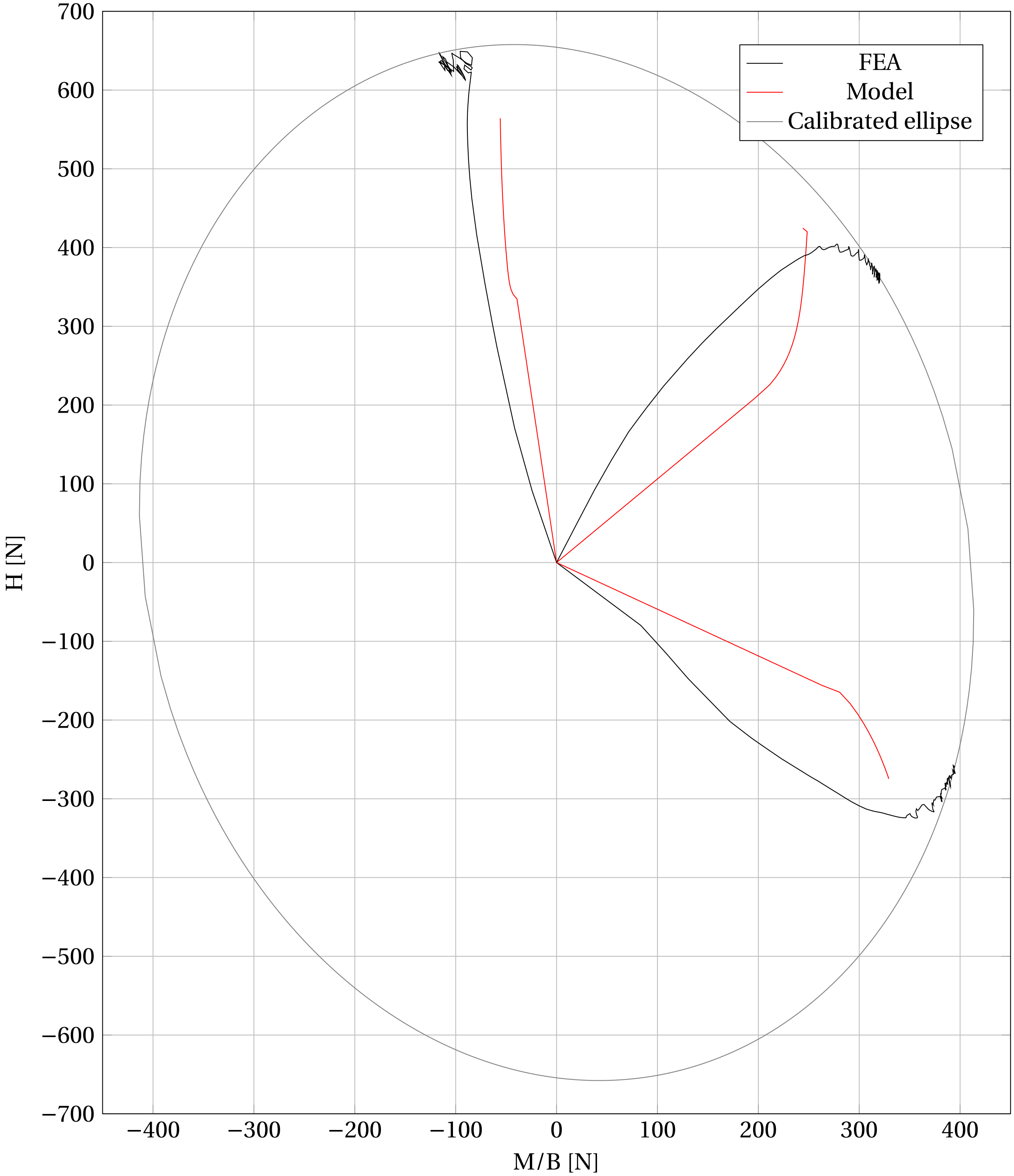

Figure 6.9: M/B-H tests with V=1000N

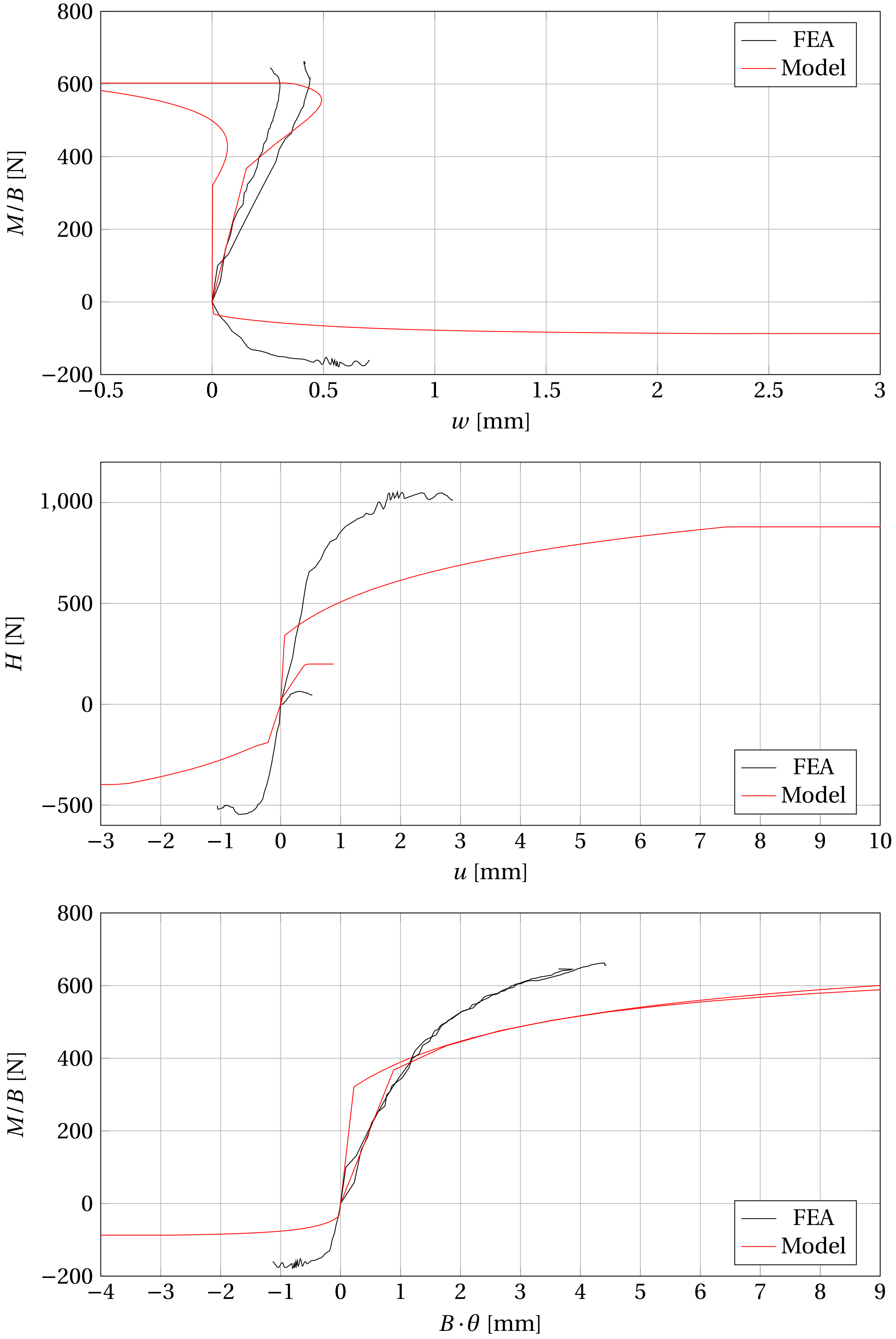

Figure 6.10: Comparison between FEA and the macro-model at V=2kN

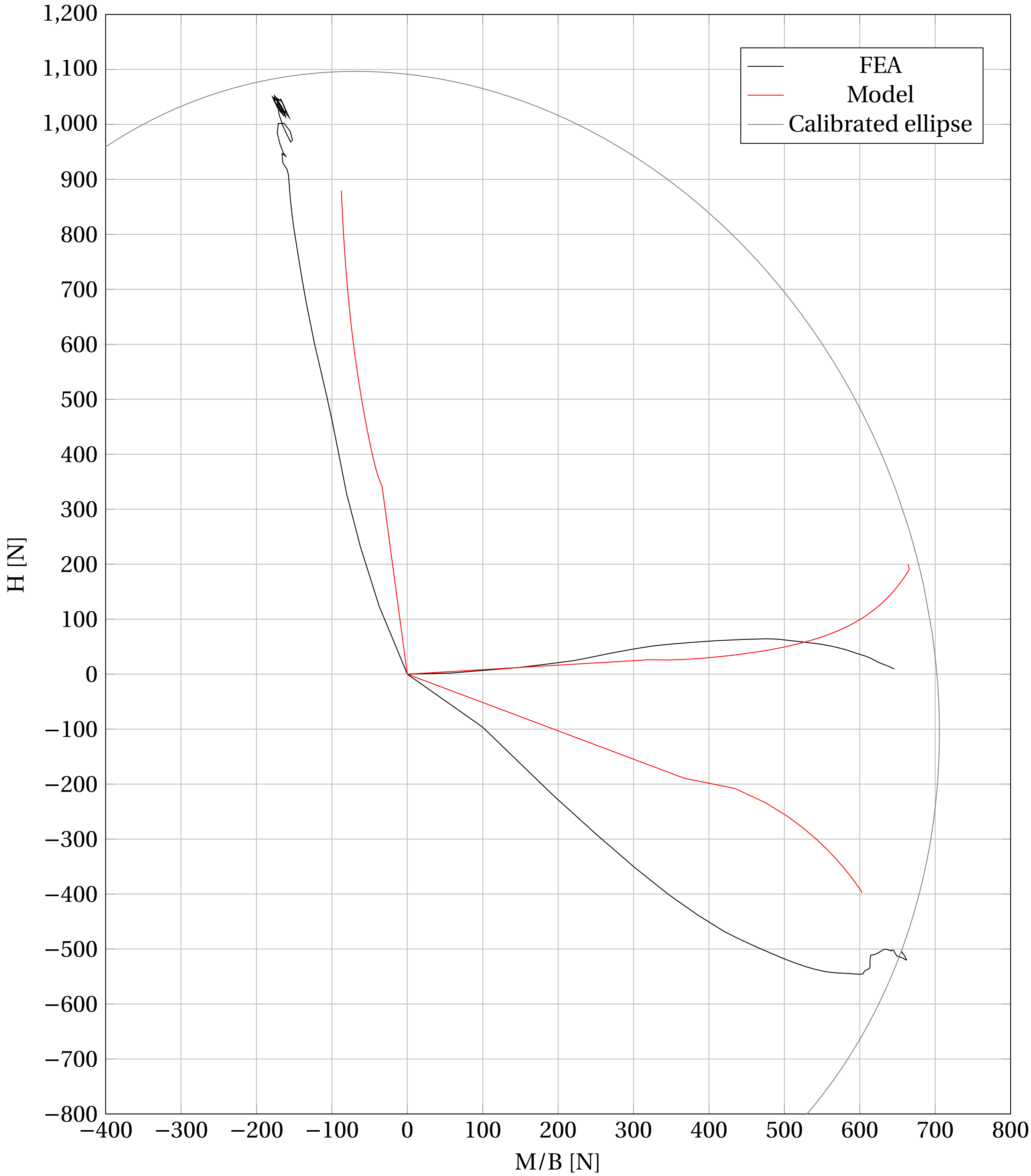

Figure 6.11: M/B-H tests with V=2000N

both for the Plaxis-results and the model-response. However when $M/B \simeq 0.3V$. Interestingly uplift was also observed for the

6.7 Calibated values

Table 6.2: Calibrated macro-model parameters

Yield surface		Potential surface		Elastic parameters		Hardening	
h_0	0.1	h_{0p}	0.35	k_1	2.56	κ_0	0.25
β_{1h}	0.83	β_{1hp}	0.01	k_2	0.47	a_h	45
β_{2h}	0.98	β_{2hp}	0.5	k_3	1.96	C_1	0.3
m_0	0.09	m_{0p}	0.16	k_4	0	C_2	0.4
β_{1m}	0.92	β_{1mp}	0.99	G	8.3 MPa		
β_{2m}	0.99	β_{2mp}	0.8				
a	-0.1	a_p	0				
V_{max}	14.5kN						

Chapter 7

Comparison with the macro-model

In this chapter the results obtained from the prototype-tests in the sand-bin are compared with those of the calibrated macro-model. This is done with the aim of validating the macro-model. The test-procedures are presented in Section 4.3, and will not be repeated. Herein only tests in the M/B-H plane are presented.

7.1 Overview

Presented first are the two sets of M/B-H tests done with the prototype-foundation and the best-fit ellipse for these tests. Both of the ellipses are similar in shape: An axis ratio of 1.6 and a counter-clockwise rotation of 10 degrees. A suggested a-value, whose value accounts for the ellipsis-rotation, is -0.16 on the basis of Equation 6.1.

Tests are compared which should be equal because of their rotational and horizontal increments applied in the combined tests done in the M/B-H plane. Three tests are compared while the vertical load is 1kN and three are done while it is 2kN. The results presented in the M/B-H planes are compared with the suggested ellipses.

7.2 Comparison between the macro-model and the prototype-tests

In the following are diagrams comparing the mechanical behavior. The rotational and horizontal increments applied are listed in Table 4.1.

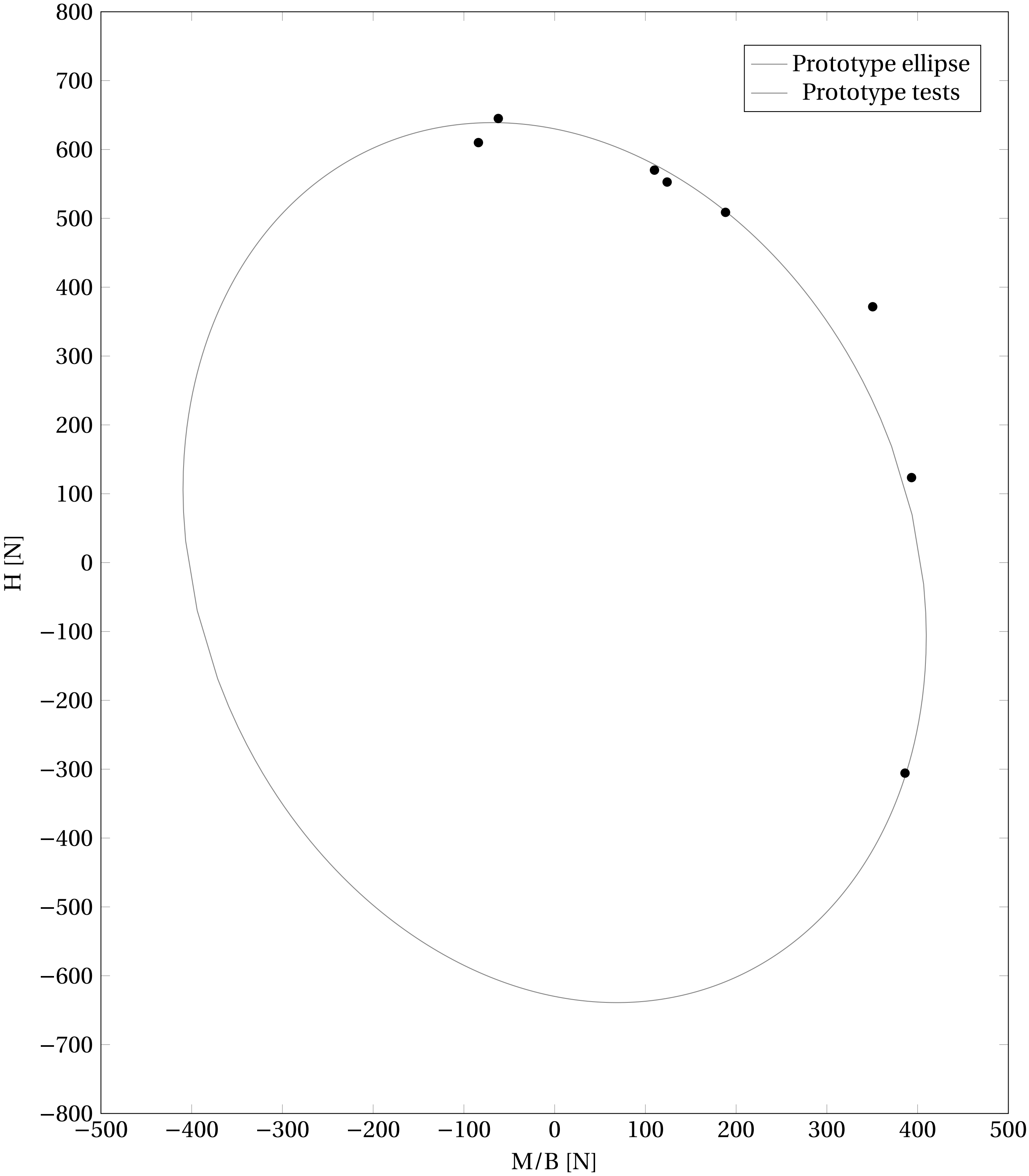

Figure 7.1: Prototype-tests and suggested ellipse in the M/B-H plane, V=1kN

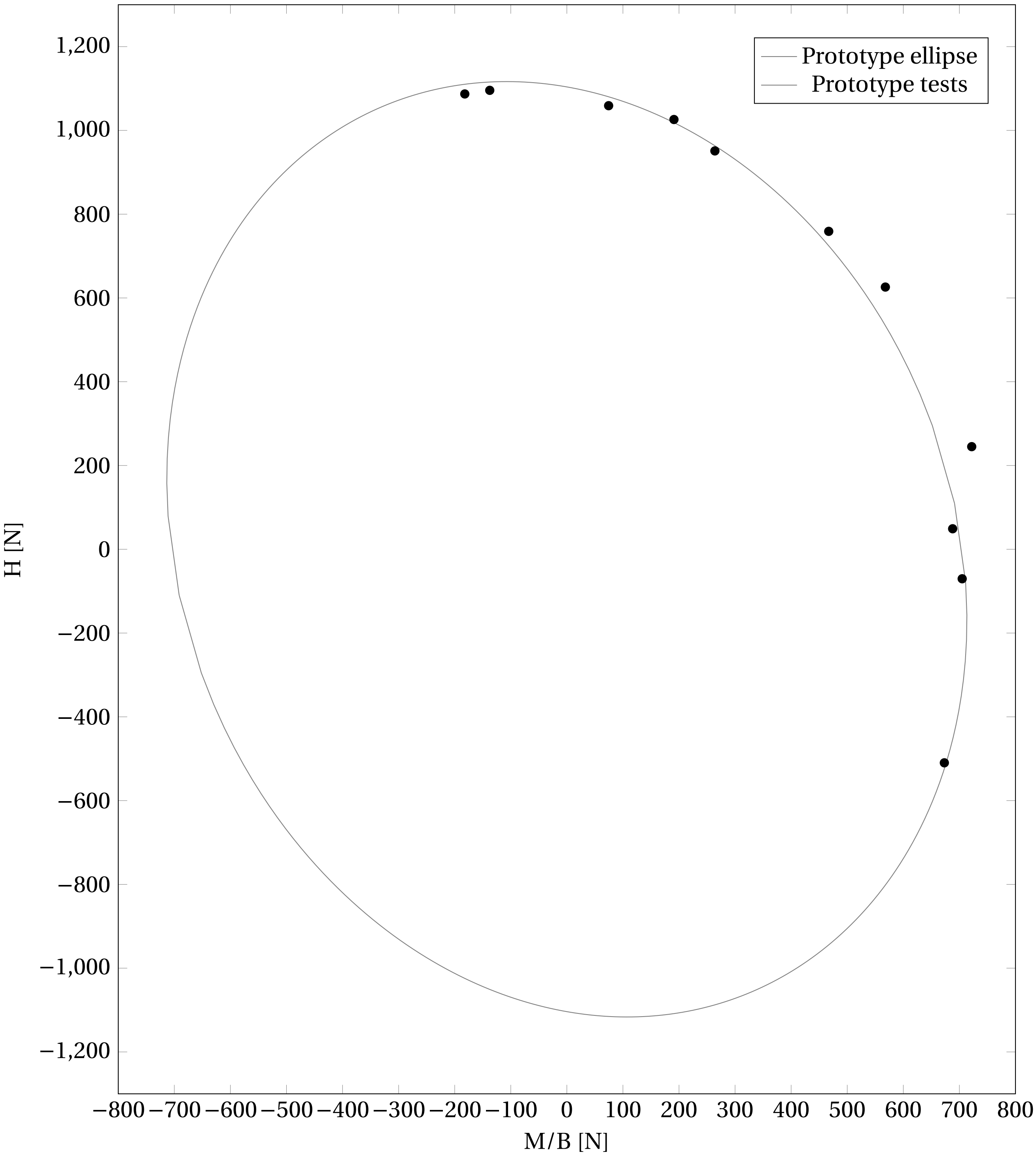

Figure 7.2: Prototype-tests and suggested ellipse in the M/B-H plane, V=2kN

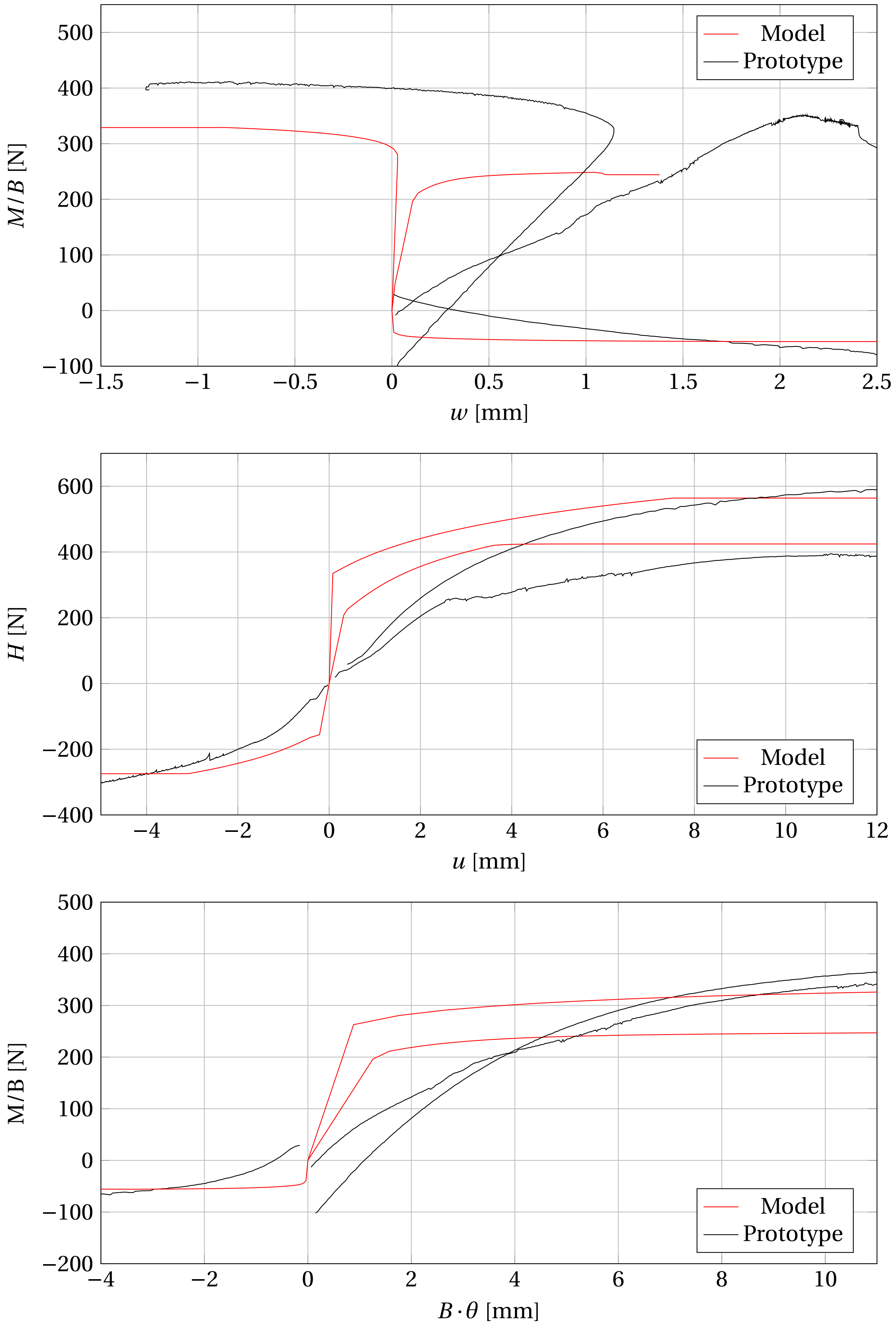

Figure 7.3: Comparison between macro-model and prototype-tests at V=1kN

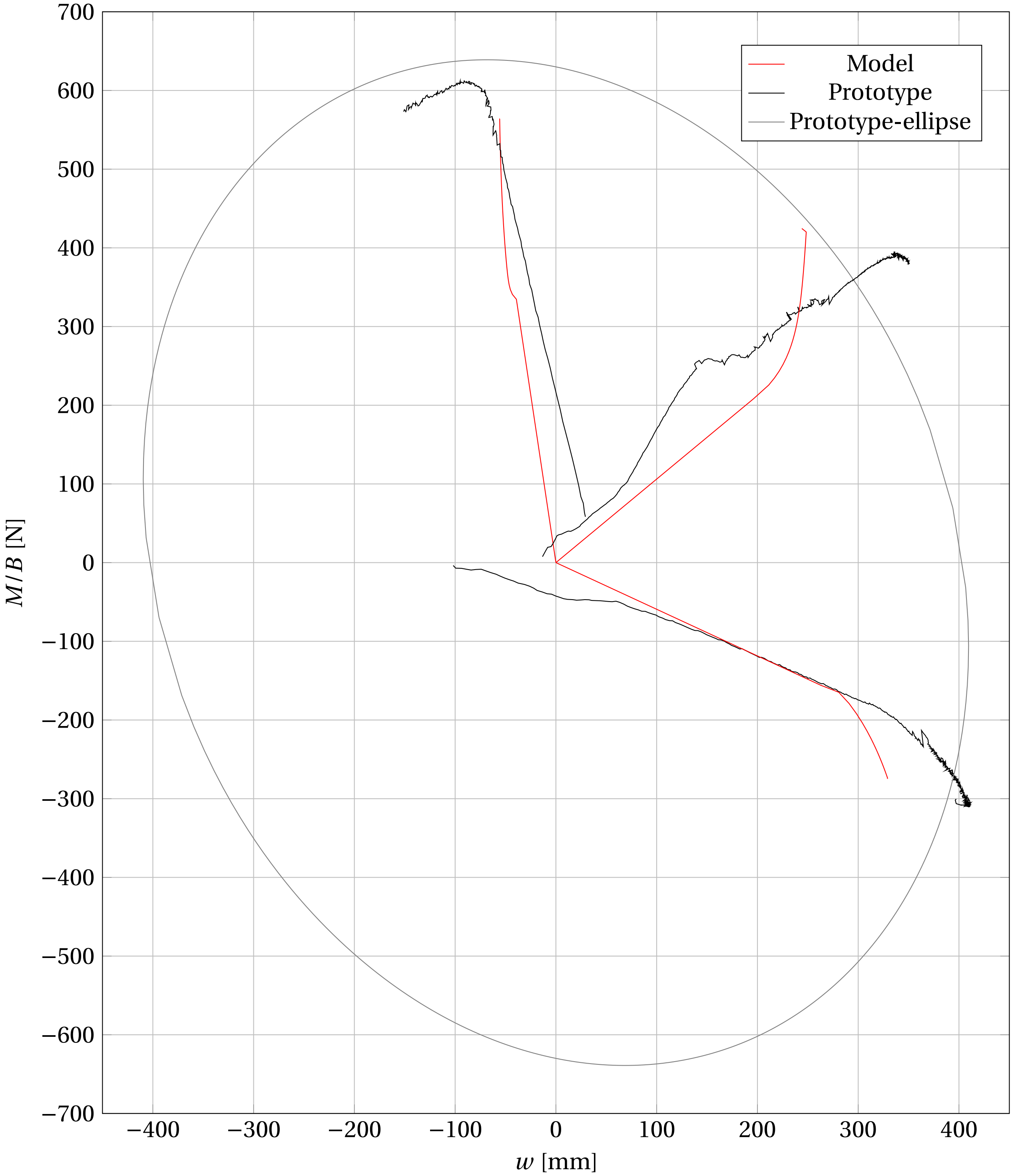

Figure 7.4: Tests in the M/B-H plane, V=1kN

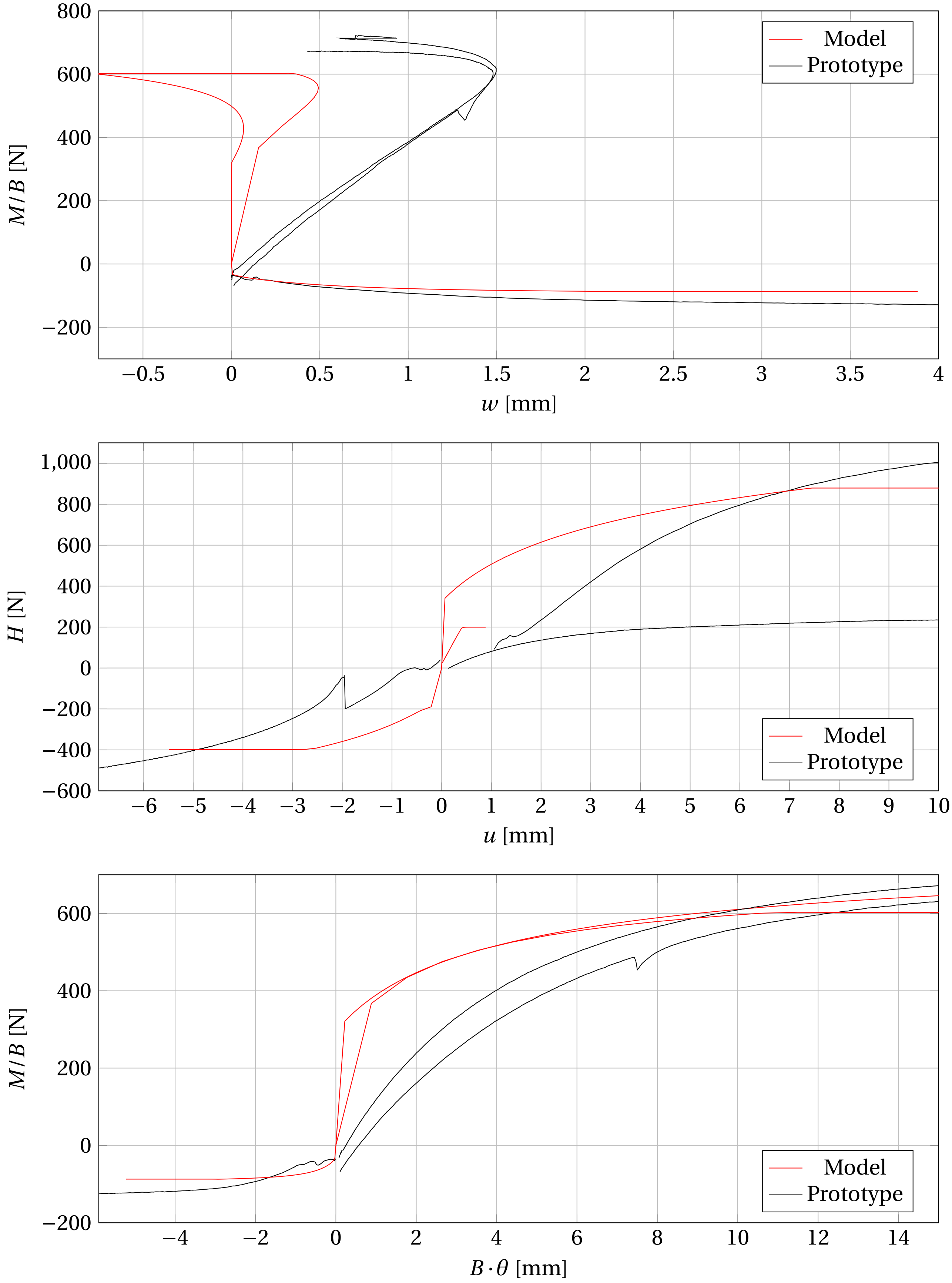

Figure 7.5: Comparison between macro-model and prototype-tests at V=2kN

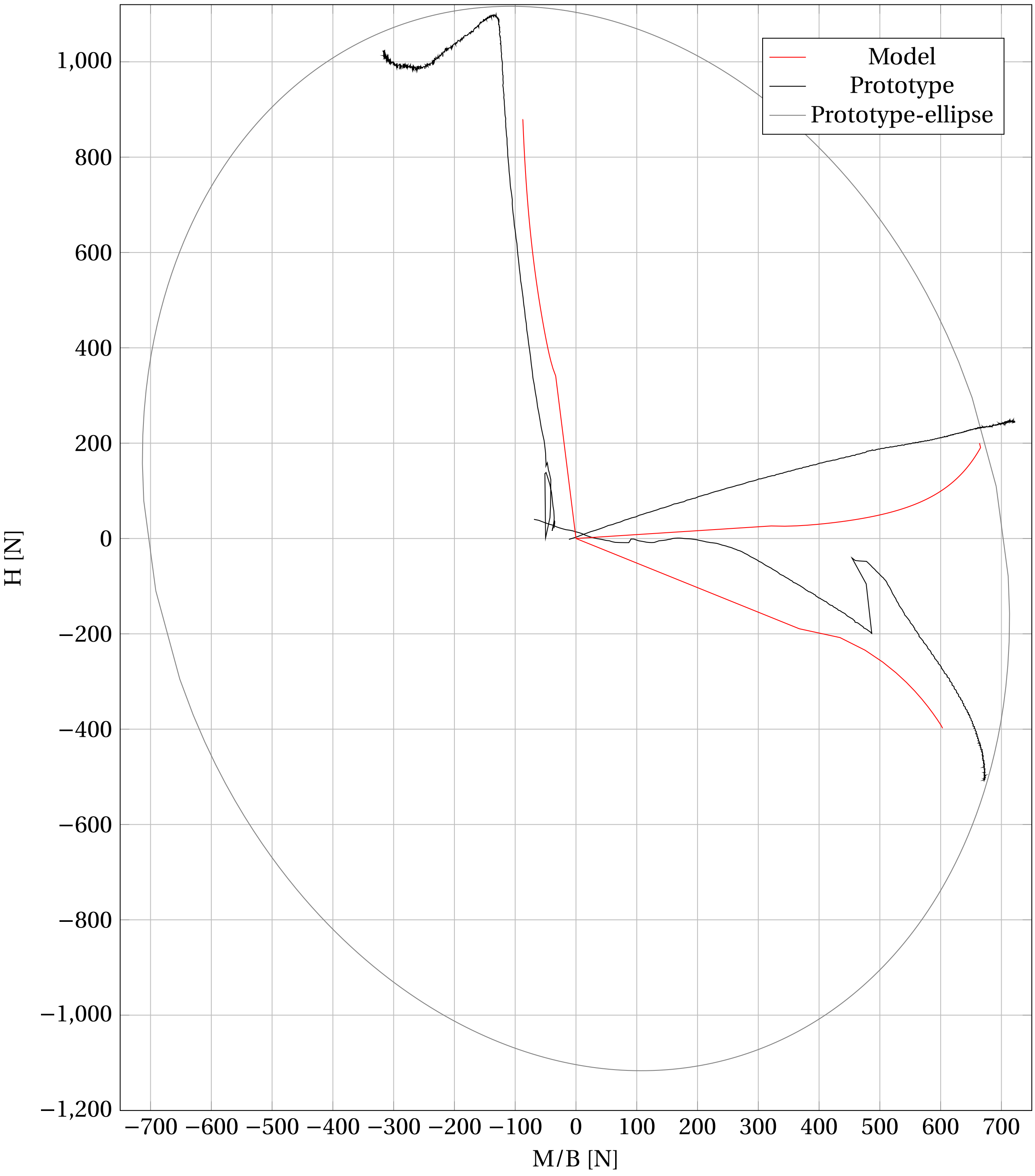

Figure 7.6: Load paths in the M/B-H plane for V=2kN

Chapter 8

Discussion, Summary and Recommendations for Further Work

In this chapter the results obtained by finite elements, the calibrated macro-model and the prototype-foundation are compared. Thence, the performance of the macro-model is discussed and to which extent it is applicable for describing the SSI between large shallow foundations and soil.

8.1 Discussion

8.1.1 General about the prototype-tests

The compared data presented were all based on the displacement ratios from the ball-screws. However, for the prototype test the load paths are also dependent on the start-point of the test. Hardly any of the prototype tests are starting in the origin, and thus (V, M/B, H)≠(V, 0, 0).

The initial eccentric loading can be caused by different things. The rigid steel box should ideally stand perfectly orthogonal on the even sand. A leveler was used to make sure the steel box was leveled at the start of the tests. However, the evenness of the sand was obtained by a vacuum-cleaner and it was difficult to obtain a perfectly even sand-surface. Although most test show small eccentric forces at the start of the tests, some did not.

The displacement ratios were chosen to investigate certain points of failure along the ellipse in the M/B-H plane. When the initial moment and horizontal forces were different from zero it was more difficult to control the load path to the place on the ellipse where it was expected of failing. The fact that few prototype-tests started in the origin in the M/B-H plane are assumed not to be too important, besides less control of the tests (assuming the initial accumulation of plastic displacements are insignificant). The failure points are therefore assumed to be reasonable.

8.1.2 Discussion regarding capacity

The vertical bearing capacity for the given geometry is higher for the FEA than for the classical bearing capacity formulae. Ideally, an analysis should be done in Plaxis 3D as this problem is in fact of a 3D nature.

What can be seen from all model-simulations is that they are not managing to reach the same failure loads as the results from Plaxis 2D or the prototype-tests in the M/B-H plane. The maximum capacity of the macro-model in the V-M and V-H planes are solely calibrated from swipe tests done in Plaxis. Interestingly, the swipe tests in e.g. the V-H plane and tests of combined control in the M/B-H plane lead to different capacities.

This variation could be due to the fact that the horizontal swipe tests have zero moment, and a slightly higher horizontal load is applicable for a small negative moment. The difference from e.g. maximum horizontal capacity for 1kN is too big to be attributed to the lack of a small moment working. The different horizontal capacities for a vertical load of 1kN are outlined in Table 8.1.

FE swipe	FE M/B-H	Prototype
560 N	650N	650N

Table 8.1: Maximum horizontal capacity for a vertical load of 1kN

The incremental shear from horizontal swipe is shown in the figure below. The shear zone-geometry is distinct, and it can thus be assumed to be at failure.

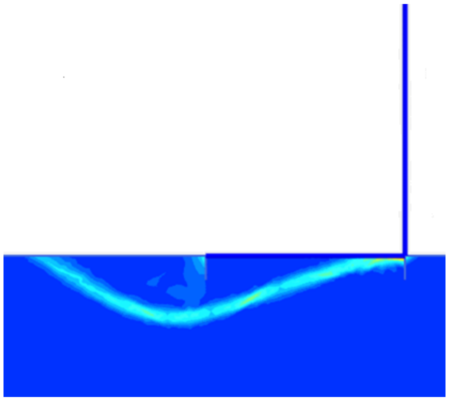

Figure 8.1: Incremental strains at a vertical load of 1kN from the horizontal swipe test

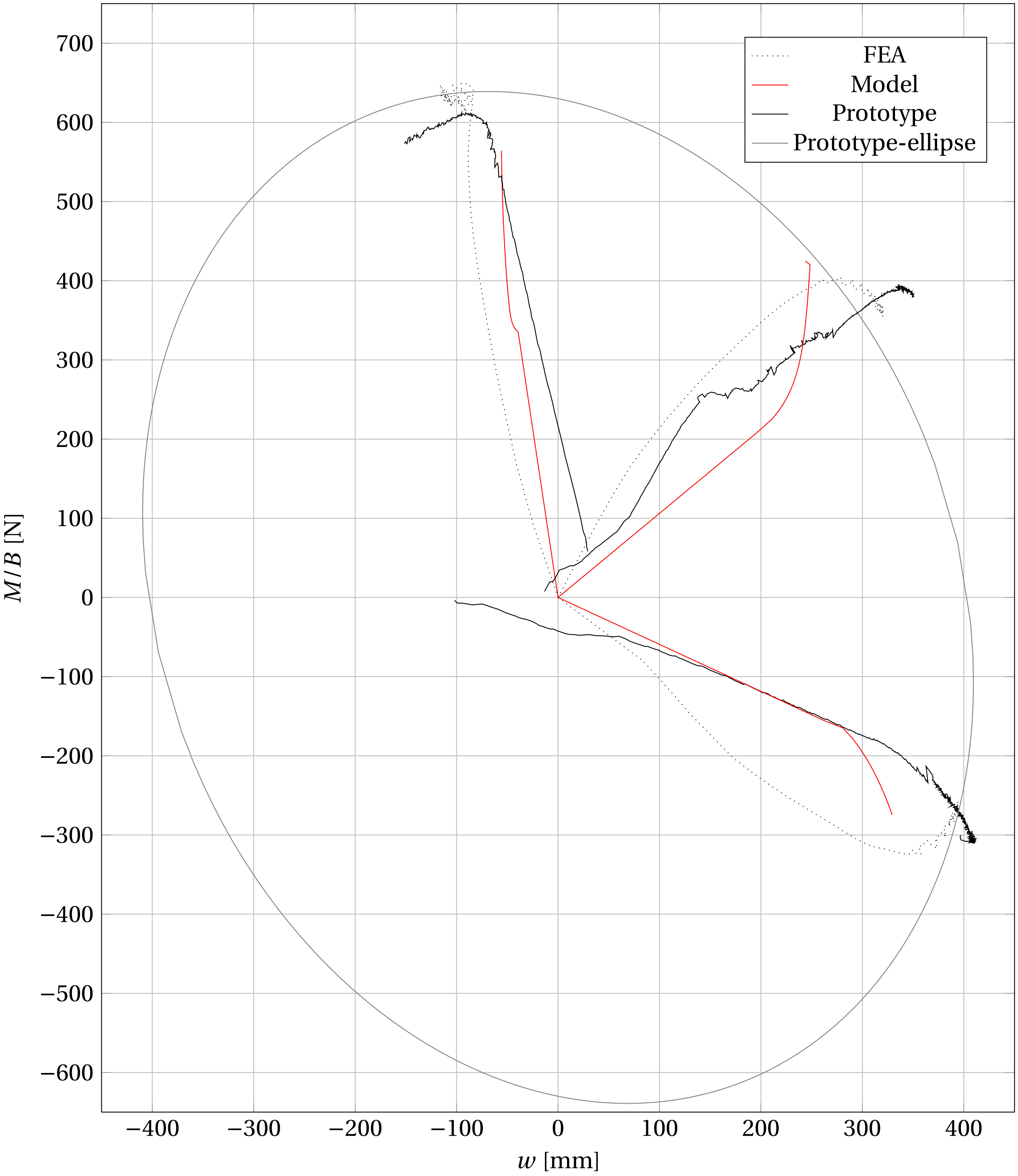

Figure 8.2: Comparison between FEA, macro-model and prototype-tests at V=1kN

In addition, two swipe test were done with the prototype-foundation. The yield-surface is only investigated at lower vertical loads due to the limitation of the test facilities not allowing for further loading than 2.5kN. The prototype-results indicate a linear initial sliding in the V-H

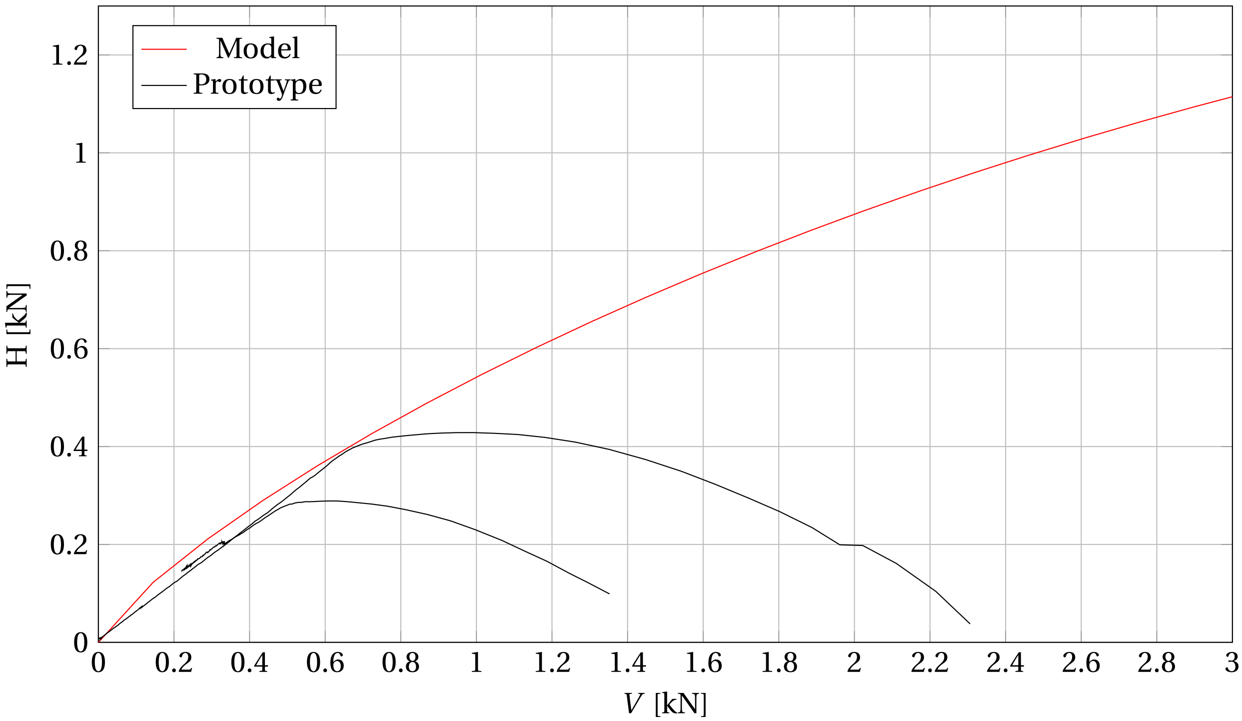

Figure 8.3: Comparison of horizontal swipe

plane, which is reasonable as the observed prototype-foundation was in fact sliding. This initial linearity is not taken into account by the calibrated yield-locus, and for large vertical loads it is not important to do so either. However, if relatively low vertical loads are important the yield surface could be reformulated to better account for this.

Therefore, the tests conducted gives the initial slope in the V-H plane, with a sliding coefficient tanδ corresponding to 0.63. Assuming zero cohesion, the in-situ interface roughness is approximated to $r = tan\delta / tan\phi$=0.78. In the finite-element analysis the roughness ratio at the interface was set to 1, on the basis of the sand glued underneath the steel-box foundation, as was mentioned in Section 4.2. This seems to have worked with some success. Either way, the roughness ratio was set to 1 in the FEA and can thus not be held accountable for a seemingly too low horizontal load during swipe.

If the initial slope indicated by the prototype-tests is assumed to continue linearly up to the vertical load of 1 kN the corresponding maximum horizontal load is approximately 650N, which is exactly what was obtained in the M/B-H tests in Plaxis and by the prototype-foundation. Yet again, this seems reasonable.

Which raises the question: why the big difference in horizontal load? These results stem both from the same Plaxis-configuration, the same soil model, the same soil-parameters and same mesh. At the same time, the higher horizontal capacity reached in the M/B-H plane are coinciding with the capacity obtained with the prototype-foundation(650N). Therefore, doubt is sown regarding the possibility of directly investigating the maximum capacity from swipe tests conducted in Plaxis 2D. They certainly give valuable information about the shape of the yield-surface, but it seems like the swipe tests are not able to accurately model the maximum capacity. It is therefore concluded that the use of swipe tests in Plaxis should be done with caution.

When the foundation is at failure in Plaxis, and further horizontal displacement is imposed a new failure configuration is required. However, to get from one failure configuration to another the soil is subject to unloading some places, while a reloading takes place elsewhere in the soil medium. There is loss of stiffness some places, while other places the stiffness increases, changing with each failure mode. The algorithms implemented in Plaxis might not be optimized for this kind of sudden change in failure configuration, which happens with each load-step at failure. This might cause the suggested inability to model maximum capacity with swipe-tests accurately in Plaxis.

Analogously, the same argument can be repeated for the case of swipe in the V-M plane. Larger moment capacity is obtained by combined controlled tests in the M/B-H plane by Plaxis than by swipe in the V-M plane by Plaxis. The same reasoning applies here, without the need to repetition.

The macro-model's capacity in the V-H and V-M/B planes are calibrated on the basis of the horizontal- and vertical swipe tests in Plaxis alone, which are criticized for seemingly being inaccurate. This can explain why the capacity is underestimated for the load-paths in the M/B-H plane for the macro-model.

8.1.3 Discussion regarding yield surface shape in the M/B-H plane

On the basis of the conducted FEA presented in Section 6.2.1 the rotation of the ellipse in the M/B-H plane is 6 degrees an axis ratio of 1.6. Similar results were obtained from the prototype-foundation tests with the same axis ratio, but with an angle of 10 degrees. This lead the ellipse-rotation factor a to go from -0.1 for the FEA to -0.16 for the prototype-test. The latter is considered more reliable.

The difference in rotation could be due to the fact that the soil geometry in Plaxis (small deformations are assumed) is not updated during loading, while the physical soil below the prototype-foundation obviously is. Another option is insecurity regarding the soil-parameters used in Plaxis.

For comparison it can be noted that Butterfield and Gottardi (1994) did similar laboratory tests on dense sand and got a rotation of 13 degrees and axis ratio of 1.64. Moreover, Butterfield and Gottardi did similar test at a vertical corresponding to approximately half of the maximum, while the tests presented in this thesis did so for vertical loads of about 10-15% of maximum vertical capacity. The rotation might be different due to different soil. The model-sand have a relative density around 65%, while the sand Butterfield and Gottardi tested had 85%. Speculation can be done regarding what causes the extent of rotation and axis ratio, but further tests are necessary to conclude. However, the results obtained seem reasonable.

8.1.4 Discussion regarding mechanical behavior in the M/B-H plane

The calibration of the presented model is done with finite elements. The potential surface is calibrated with curve-fitting with the macro-model. From Figure 6.8 it is apparent that there is uplift behavior from Plaxis for one of the load-combinations, while for the macro-model and prototype-foundation it is not. When calibrating it was clear that the potential surface could be altered to accommodate for uplift for this load-combination with the macro-model. However, this would have meant worse fit for the other load-combinations and a compromise was made: the model did not reproduce the uplift-behavior as Plaxis did for this load-combination. The prototype-test does not show any uplift either, and the compromise seems reasonable. The potential parameters chosen gave overall reasonable results.

The comparison between results from the FEA, the macro-model and the prototype-testing is done in Figure 8.4. When the load-combination is within the yield surface the soil acts elastic. Clearly, the elastic stiffness is too high as can be seen from both the M/B-w, H-u and M/B-Bθ diagrams shown in Figure 8.4. This can be due to either the dimensionless diagonal terms in the elastic stiffness-matrix being too large, or the elastic shear modulus G being too large. The dimensionless diagonal terms are totally general for the geometry given (the major side of the foundation being twice as long as the shorter). The stiffness terms are described thoroughly in the literature, and Table 6.1 shows that 4 authors virtually obtain the same stiffnesses.

The stiff behavior is therefore attributed to the shear modulus G. It is reasoned in Section 6.3 that a representative stress level of the shear modulus is approximately 8kPa. The chosen shear modulus is suggested by assuming that the initial stiffness E_0 at 20 kPa confining stress is the same at a lower stress. A questionable assumption, in retrospect. The initial stiffness from this test suggest 22MPa, and by assuming a Poisson' ratio of 1/3, the shear modulus becomes 8.3MPa. Unfortunately, it was realized that the shear modulus was too stiff too late for it to be changed in the analysis. Moreover, a change in the shear modulus will also have consequences for the hardening law due to the way the plastic increments are extracted($d\boldsymbol{v}^p = d\boldsymbol{v}^{tot} - d\boldsymbol{v}^e$).

When the soil acts plastic the kinematic behavior seems reasonable. Uplift behavior is accounted for at M/B-values at approximately 0.25V. This was emphasized in Section 6.5 to be important.

The potential surface and hardening law are governing the evolution of plastic behavior. Seven parameters are defining the shape of the plastic surface. It could be argued that the curve-fitting procedure for calibrating the potential surface is somewhat questionable. However, calibrating it analytically is no easy task. Furthermore, the basis of such an analysis would be to extract the increments from Plaxis. These would need to be compared with the analytically obtained plastic increments, which in turn are dependent on the potential surface.

At material yield and evolution of plastic displacement the consistency condition ensures that dF=0. Thus, the point (V, M/B, H) stays on the yield surface during plastic yielding. A short derivation of the analytic expression for such an increment is given:

$$dF = \frac{\partial F}{\partial \mathbf{S}} \cdot d\mathbf{S} + \frac{\partial F}{\partial V_0} \cdot dV_0 = 0 \tag{8.1}$$

$$dF = \frac{\partial F}{\partial \mathbf{S}} \cdot \mathbf{D} \cdot d\mathbf{v}^{\mathbf{e}} + \frac{\partial F}{\partial V_0} \cdot \frac{\partial V_0}{\partial \kappa} \cdot \frac{\partial \kappa}{\partial U_p} \cdot \frac{\partial U_p}{\partial \mathbf{v}^p} \cdot d\mathbf{v}^p = 0 \tag{8.2}$$

$$dF = \frac{\partial F}{\partial \mathbf{S}} \cdot \mathbf{D} \cdot \left[d\mathbf{v} - d\mathbf{v}^{\mathbf{p}} \right] + \frac{\partial F}{\partial V_0} \cdot \frac{\partial V_0}{\partial \kappa} \cdot \frac{\partial \kappa}{\partial U_p} \cdot \frac{\partial U_p}{\partial \mathbf{v}^p} \cdot \frac{\partial Q}{\partial \mathbf{S}} \cdot d\lambda = 0 \tag{8.3}$$

which leads to the scalar dλ being:

$$d\lambda = \frac{\frac{\partial F}{\partial \mathbf{S}} \cdot \mathbf{D} \cdot d\mathbf{v}}{\frac{\partial F}{\partial \mathbf{S}} \cdot \mathbf{D} \frac{\partial Q}{\partial \mathbf{S}} - \frac{\partial F}{\partial V_0} \cdot \frac{\partial V_0}{\partial \kappa} \cdot \frac{\partial \kappa}{\partial U_p} \cdot \frac{\partial U_p}{\partial \mathbf{v}^p} \cdot \frac{\partial Q}{\partial \mathbf{S}}} \tag{8.4}$$

The flow rule requires that the plastic increment is the following:

$$d\boldsymbol{v}^{\boldsymbol{p}} = d\lambda \cdot \frac{\partial Q}{\partial \boldsymbol{S}} \tag{8.5}$$

Hence, all the ingredients for determining the plastic increment are in place. The plastic increments from the FEA are compared with those obtained analytically, whose values should not deviate much from one another. The introduction of an algorithm minimizing the error between the extracted plastic increments from the FEA and the analytically obtained plastic increments could lead to more well-suited potential parameters than the ones chosen in this thesis. A limited amount of time led this option not to be considered further. However, the plastic soil behavior is reproduced adequately.

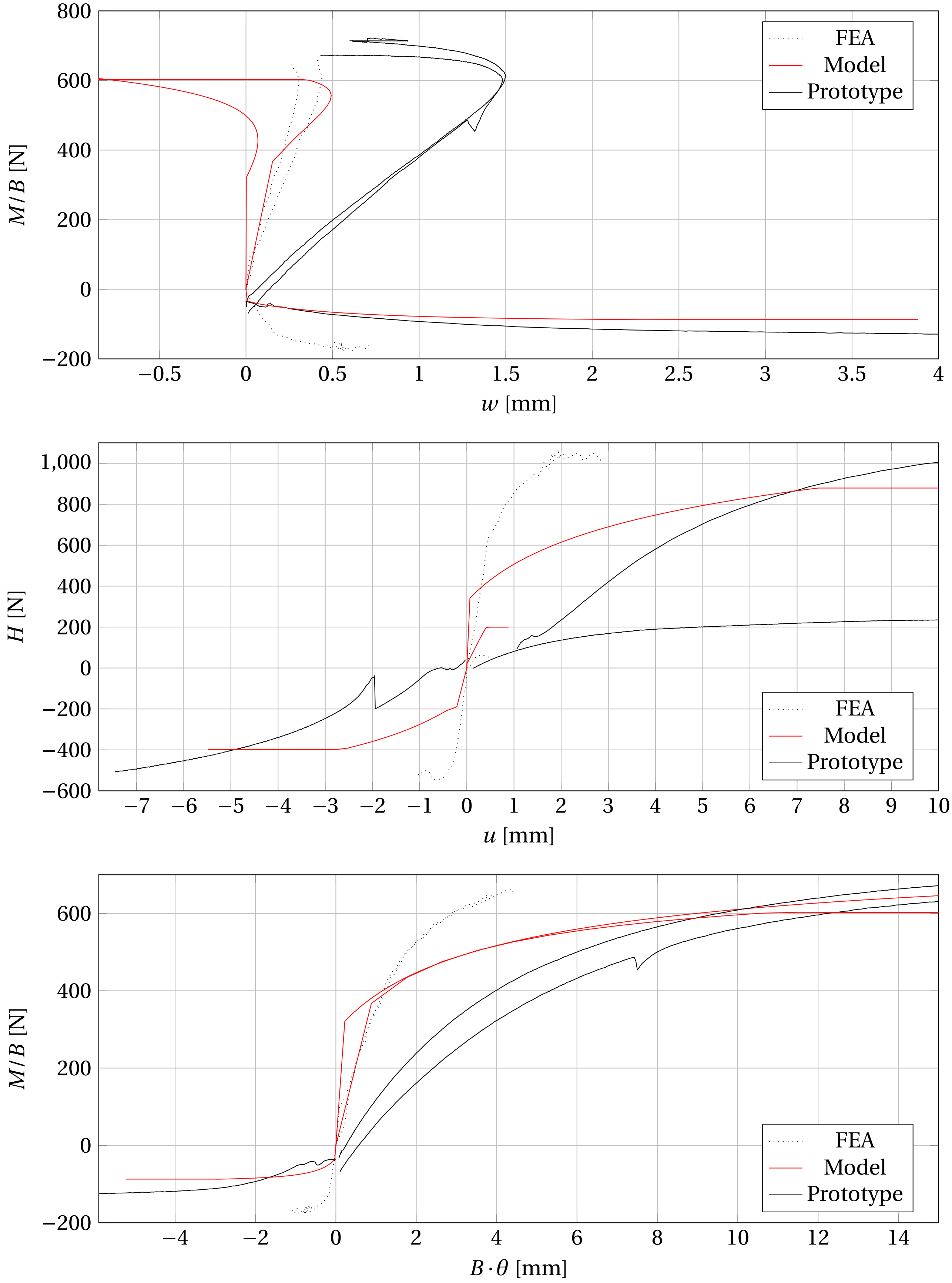

Figure 8.4: Comparison between FEA, macro-model and prototype-tests at V=2kN

8.1.5 Discussion regarding the hardening law

If the shear modulus is changed, consequently the hardening law-parameters are changed as well. The plastic increments extracted from the FEA are dependent on the chosen shear modulus, as can be seen in Equation 6.1. Thence, the development of the combined plastic displacement U_p is changed. If the shear modulus is reduced, then the elastic incremental displacement are larger, and thus the plastic incremental displacements are smaller. Therefore, the development of the combined plastic displacement would evolve slower.

The chosen hardening law relation is bi-linear on the basis of the idealized plastic combined displacement extracted from the FEA. However, as pointed out earlier the trend is highly dependent on load-combination. The trend might be bi-linear for H/(M/B)-ratios close to 1, but when this ratio increases, i.e. when the horizontal load becomes more dominant the observed trend becomes less linear. This is apparent exemplified in the figure below. The figure to the left have a ratio H/(M/B) of 1.15, while the one to the right 6.6.

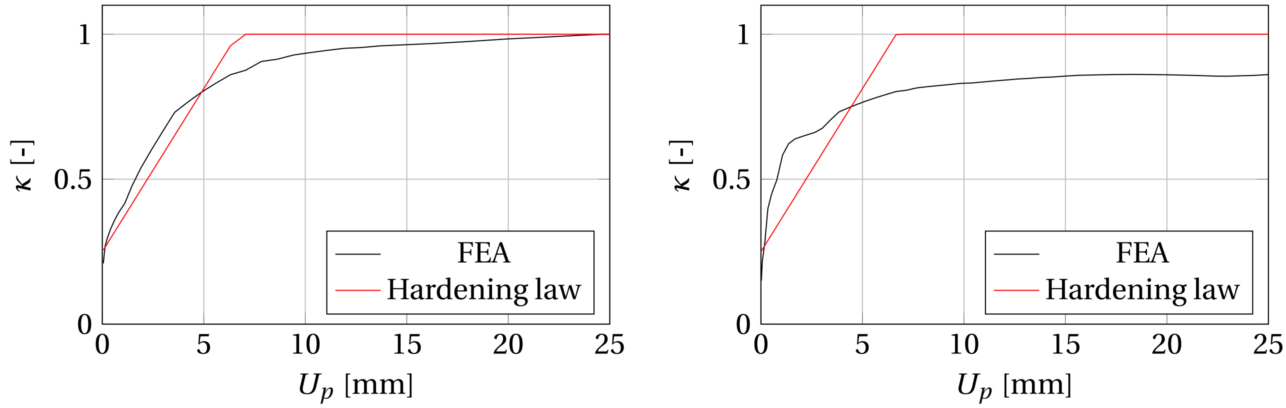

Figure 8.5: State parameter vs combined plastic displacement for two load-combinations

It could therefore be convenient to introduce a different hardening-relationship if load-combinations with H/(M/B)-ratios far from 1 are important. One such example could be a hyperbolic hardening relation.

8.1.6 Discussion regarding triaxial results

HS-parameters are found on the basis of two triaxial tests relatively close in confining stress-range, i.e. 20 and 30 kPa. These results compare very well. However, for FEAs with lower stress ranges, the corresponding stiffnesses are extrapolated from triaxial results with higher confining stress. The figure shown below is a typical test in the M/B-H plane for a constant vertical load of 2kN. The average minimum principal stresses are approximately 14kPa. For a vertical loading of 1kN the average minimum principal stresses are lower. Ideally, tests with lower confining stresses should have been done.

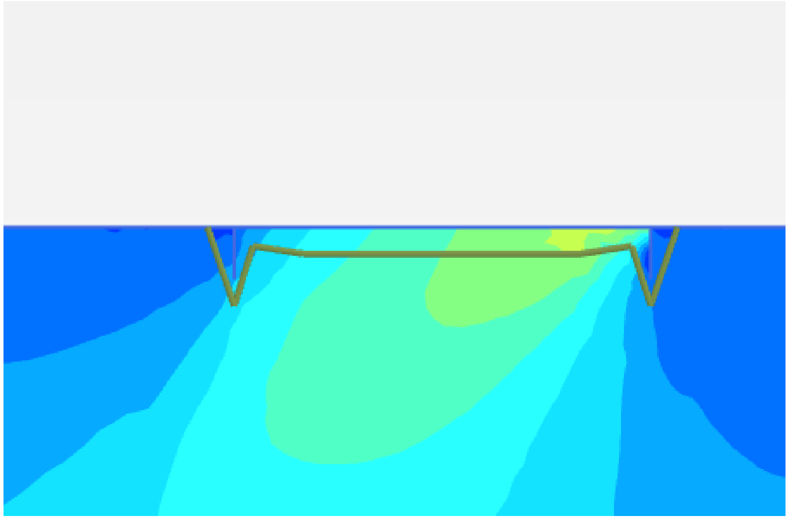

Figure 8.6: Typical load-combination and the development of stress. M/B-H plane with constant vertial load of 2kN

8.1.7 Discussion regarding up-scaling procedure

The only geometry investigated within this thesis is a rectangular foundation with lengths 0.4 and 0.2 m. The soil is described within Chapter 4. If the studied model is to be coupled with a structure-analysis an up-scaling procedure must follow. The constitutive relationship presented herein is related to two different categories of parameters: the geometry and the soil-stratification. The constitutive relationship is however totally general, and can be adapted to fit different geometries and soil-profiles.

The macro-model framework presented within this thesis can therefore be adopted for any kind of large shallow foundations with rigid behavior with respect to the soil. In essence, that would mean most large shallow foundation, e.g. GBS-foundations anchoring suspension bridge cable.

Important characteristics regarding the mechanical behavior is investigated in the test-chamber. Scale-effects, if any, can be studied with large-scale testing, or centrifuge swipe testing, as argued by Gottardi and Govoni (1995).

8.2 Summary

The performance of a presented macro-model is studied. The model is calibrated with finite elements and validated with prototype tests. Index- and triaxial tests are conducted to get representative parameters for the Hardening Soil-model, which is used for calibration in Plaxis.

It is emphasized that the model's ability to reproduce the mechanical behavior is important, especially its ability to reproduce uplift behavior for large moments. Comparison with prototype-testing for similar load-combinations show that the macro-model is able account for uplift.

The model and its theoretical formulation seems well-suited for large foundations subject to eccentric forces. The overall reproduction of the mechanical behavior seems satisfactory for the small-scale foundation investigated, although some modifications are suggested. The elastic stiffness is somewhat high (attributed to a high shear modulus), and the capacity in the M/B-H plane is slightly underestimated.

Application at Bjørnafjorden, and inclusion of the macro-element in the structural analysis can be done. Moreover, the macro-model framework presented herein is general, and can thus be adapted to other geometries and soil-profiles.

8.3 Recommendations for further work

8.3.1 Updated shear modulus

Comparison with the prototype-tests show that the behavior in the elastic regime is generally too stiff, due to the shear modulus. The issue of determining a better suited shear modulus can be approached through FEA and the ”unit-load method”.

By doing an elastic analysis in Plaxis 3D, and impose unit displacements to the foundation associated with the three stiffness terms, the reactions can be extracted. The reactions should equalize the terms on the right side of the equation stated below. This must necessarily be an iterative process. The first iteration is suggested as the following.

A new value of G is suggested, through the stress-dependent stiffness analogy of the Hardening Soil-model. The E_{50} is assumed to be a representative elastic Young's modulus. The E_{50}-value is dependent on the $\sigma_3^{'}$ -stress, and a $K_0^{'}$ of 0.36 ($K_0^{nc} = 1 - sin\phi$) is assumed. The minimum principal stress is assumed to be approximately 8kPa as argued in Section 6.3

Therefore, $E_{50} = E_{50}^{ref}(8kPa/100kPa)^{0.4} = 10MPa$ and in turn the new suggested G is $G_{50} = E_{50}/2(1+0.33)$ which is 3.8 MPa.

When the terms on the right and left side of the equation are practically equal, the G chosen for the elastic soil stratum is chosen as the shear-modulus of the macro-model.

$$\begin{bmatrix} dV \\ dM/0.4m \\ dH \end{bmatrix} = G \cdot 0.4m \begin{bmatrix} 2.56 & 0 & 0 \\ 0 & 0.47 & 0 \\ 0 & 0 & 1.96 \end{bmatrix} \begin{bmatrix} dw^e \\ 0.4m \cdot d\theta^e \\ du^e \end{bmatrix} \tag{8.6}$$

8.3.2 Further model-validation

As pointed out earlier there has been done test at vertical loads, approximately 15 % of maximum vertical bearing capacity. More tests to further validate the macro-model and to investigate if it performs well also for vertical loads closer to vertical capacity would be interesting. There are two alternatives, either a higher vertical force is applied by e.g. a hydraulic jack, or the area of the foundation is decreased. The maximum vertical capacity of the presented test-facility is 2.5 kN. However, for the tests to be comparable the same relationship between the major and minor side of the rectangular foundation must be kept constant, i.e. 2. Generally, the geometry can be different, but for comparison with the tests done it is convenient to keep the same foundation shape.

The bearing capacity of Brinch-Hansen suggests that a foundation-geometry with lengths of 7.5cm and 15cm the maximum vertical capacity is approximately 50kPa. The maximum possible stress induced in the sand-bin is then 220kPa, and the soil can thence be driven to vertical failure. More geometries tested means a better understanding of the capacity. Centrifuge and large-scale tests would also increase the understanding of potential scale-effects.

Throughout this thesis all diagrams have referred to loads in either N or kN. When a different foundation-geometry is tested it is more convenient to normalize all loads, e.g. by dividing all loads by the maximum vertical capacity for the specific foundation geometries.

8.3.3 Extension of the model

For a suspension bridge with large cable forces a macro-model with three degrees of freedom is herein deemed sufficient. However, the model can be extended to account for loads acting whichever direction, thus extending the degrees of freedom to six (the corresponding forces are Hx, Mx, Hy, My, V and Mz). One example is Cassidy and Martin (2004), who presented a macro-model describing a jack-up foundation with general static loading in the six-dimensional space.

In rough sea, cyclic behavior is expected and can cause both a strength reduction in the soil and hysteretic behavior. The presented macro-model only accounts for static loads. However, an extension can be made to account for dynamic loading as well. The formulation presented herein would then probably need to be significantly altered, but this is possible.

Appendix A

Complementary model sand-information

In this appendix, the specific values obtained during the sand-investigation are given.

A.1 Tables

A.1.1 Grain density

m$_{dry}[g]$	m$_{pycno}[g]$	m$_{pycno+sample}[g]$	$\rho_s[g/cm^3]$	$\gamma_s[kN/m^3]$
27.84	150.64	168.26	2.724	26.723
26.56	148.993	165.36	2.606	25.62
34.66	148.938	170.23	2.593	25.435

Table A.1: Grain density results from pycnometer

A.1.2 Maximum porosity

dry mass [g]	height [cm]	$\gamma_{dry}[kN/m^3]$	porosity [%]
670.47	7.7	13.886	46.43
667.49	7.7	13.824	46.64
611.65	7.0	13.934	46.21

Table A.2: Maximum porosity results

A.1.3 Minimum porosity

dry mass [g]	height [cm]	$\gamma_{dry}[kN/m^3]$	porosity [%]
1176	8.75	16.716	35.48
1148	8.55	16.771	35.26
1272	9.475	16.768	35.27

Table A.3: Minimum porosity results

A.1.4 In-situ density

dry mass [g]	volume [cm^3]	$\gamma_{dry}[kN/m^3]$	porosity [%]
2544.6	1602.37	15.579	39.87
2531.7	1572.70	15.791	39.04
1625.8	1005.37	15.836	38.77

Table A.4: In-situ density and porosity tests

A.1.5 porosity vs. tanϕ

$\sigma_3^{'}$ [kPa]	Porosity [%]	Relative density [%]	tan$\phi[-]$
20	39.1	66.7	0.83
30	39.9	59.1	0.83
40	38.4	72.8	0.8

Table A.5: General overview of triaxial tests done, assuming zero attraction

Bibliography

Brinch-Hansen, J. (1970). A revised and extended formula for bearing capacity. *Danish Geotechnical Institute*, Belletin No.28:5–11.

Butterfield, R. and Gottardi, G. (1994). A complete three-dimensional failure envelope for shallow footings on sand. *Gètechnique*, 44:181–184.

Byrne, B. and Houlsby, G. (2001). Observations of footing behaviour on loose carbonate sands. *Gètechnique*, 51:463–466.

Cassidy, M. and Martin, C.M. andHoulsby, G. (2004). Development and application of force resultant models describing jack-up foundation behaviour. *Marine Structures*, 17:165–193.

Cremer, C., Pecker, A., and Davenne, L. (2002). Modelling of nonlinear dynamic behaviour of a shallow strip foundation with macro-element. *Journal of Earthquake Engineering*, 06:175–211.

Dominguez, J. Dynamic stiffness of rectangular foundations. Technical report, MIT(1977).

Gazetas, G. (1991). Formulas and charts for impedances of surface and embedded foundations. *Journal of Geotechnical Engineering*, 117.

Gottardi, G. and Butterfield, R. (1993). On the bearing capacity of surface footings on sand under general planar loads. *Soils and Foundations*, 33:68–79.

Gottardi, G. and Butterfield, R. (1995). The displacement of a model rigid surface footing on dense sand under general planar loading. *Soils and Foundations*, 35:71–82.

Gottardi, G. and Govoni, L. (1995). Yield loci for shallow foundations by 'swipe' testing. *Soils and Foundations*, 35:71–82.

Gottardi, G., Houlsby, G. T., and Butterfield, R. a. (1999). The plastic response of circular footings on sand under general planar loading. *Gètechnique*, 49:453–469.

Houlsby, G. and Cassidy, G. (2002). A plasticity model for the behaviour of footings on sand under combined loading. *Gètechnique*, 52:117–129.

Janbu, N., Grande, L., and Eggereide, K. (1976). Effective stress stability analysis for gravity structures. In *Behaviour of Off-Shore Structures*, volume 1, Trondheim, Norway.

Lieng, J. T. (1988). *Behaviour of laterally loaded piles in sand - Large scale model test.* PhD thesis, Norwegian University of Science and Technology.

Martin, C. M. (1994). *Physical and numerical modelling of offshore foundations under combined loads.* PhD thesis, University of Oxford.

Nordal, S. (2016). *Geotechnical Engieering, Advanced Course [Class Handout].* Geotechnical division, NTNU.

Nova, R. and Montrasio, L. (1991). A complete three-dimensional failure envelope for shallow footings on sand. *Gètechnique*, 41:243–256.

Pais, A. and Kausel, E. (1988). Approximate formulas for dynamic stiffnesses of rigid foundations. *Soil Dynamics and Earthquake Engineering*, 7:213–227.

Plaxis. *Material Models Manual(2017).*

Roscoe, K. H. and Schofield, A. N. (1956). The stability of short pier foundations in sand. *British Welding Journal*, pages 343–354.

Sandven, R. (1992). Skirt foundations. Results from the model test in sand bin. Contract No. T. 182422, SINTEF Geotechnical Engineering Report.

Tefera, T. H. (2004). *Large scale model study and numerical investigation of sheet pile wall.* PhD thesis, Norwegian University of Science and Technology.

Terzaghi, K. . *Theoretical Soil Mechanics.* John Wiley and Sons Inc. (1943).

Tistel, J. and Grimstad, G. (2016). A macromodel description of the non-linear anchor block foundation behavior. In ZINGONI, A., editor, *Structural Engineering, Mechanics and Computation Conference*, Cape Town, South Africa. CRC Press Taylor Francis group.

TNPRA (2016). The E39 Coastal Highway Route. `http://www.vegvesen.no/Vegprosjekter/ferjefriE39/English`. [Online; accessed 11-December-2016].

Ulstein, H., Skogstrøm, J., and Grünfeld, L. (2015). Produktivitetseffekter av ferjefri e39.

Wong, H. L. and Luco, J. E. Tables of impedance functions and input motions for rectangular foundations. Technical report, Univ. of Southern California(1978).

Yang, Z. X., Li, X. S., and Yang, J. (2008). Quantifying and modelling fabric anisotropy of granular soils. *Gètechnique*, 58:237–248.

Zaharescu, E. (1961). The eccentricity sense influence of the inclined load on the bearing capacity of rigid foundations. *Journal National Buildings Organization*, 6.